Title
A simulation-based efficiency comparison of AC and DC power distribution networks in commercial buildings

Journal
Applied Energy, 210(C)

ISSN
0306-2619

Authors
Gerber, Daniel L
Vossos, Vagelis
Feng, Wei
et al.

Publication Date
2018

DOI
10.1016/j.apenergy.2017.05.179

Peer reviewed

A Simulation-Based Efficiency Comparison of AC and DC Power Distribution Networks in Commercial Buildings

Daniel L. Gerber[a], Vagelis Vossos[a], Wei Feng[a,*], Chris Marnay[a], Bruce Nordman[a], Richard Brown[a]

[a]*Lawrence Berkeley National Laboratory, Building 90, 1 Cyclotron Rd, Berkeley, CA 94720*

Abstract

Direct current (DC) power distribution has recently gained traction in buildings research due to the proliferation of on-site electricity generation and battery storage, and an increasing prevalence of internal DC loads. The research discussed in this paper uses Modelica-based simulation to compare the efficiency of DC building power distribution with an equivalent alternating current (AC) distribution. The buildings are all modeled with solar generation, battery storage, and loads that are representative of the most efficient building technology. A variety of parametric simulations determine how and when DC distribution proves advantageous. These simulations also validate previous studies that use simpler approaches and arithmetic efficiency models.

This work shows that using DC distribution can be considerably more efficient: a medium sized office building using DC distribution has an expected baseline of 12% savings, but may also save up to 18%. In these results, the baseline simulation parameters are for a zero net energy (ZNE) building that can island as a microgrid. DC is most advantageous in buildings with large solar capacity, large battery capacity, and high voltage distribution.

Keywords: commercial buildings, efficiency, direct current, simulation, Modelica

1. Introduction

Recent interest in direct current (DC) power distribution systems in buildings has been spurred by a number of factors, including a rapid growth in photovoltaic (PV) system installations [1],

*Corresponding author

Email addresses: dgerb@berkeley.edu (Daniel L. Gerber), evossos@lbl.gov (Vagelis Vossos), weifeng@lbl.gov (Wei Feng), chrismarnay@lbl.gov (Chris Marnay), bnordman@lbl.gov (Bruce Nordman), rebrown@lbl.gov (Richard Brown)

the emergence of batteries in the building sector [2], and the increasing market of end-use loads operating internally on DC such as electronics, motors with variable frequency drives (VFDs), and light emitting diode (LED) lighting [3]. Direct power distribution of DC from PV systems and batteries to DC appliances can reduce power conversion losses from DC to alternating current (AC) and back, leading to electricity savings within the building power distribution system [4]. DC distribution systems have been proposed and implemented successfully in data centers, where electricity savings between 7% and 28% have been estimated for a 380 V DC distribution system compared to an equivalent system operating at 208 V AC. [5]. Commercial buildings in the United States, which currently consume 61% of their energy in electricity [6], have seen early adoption use cases for DC distribution systems, primarily in lighting applications, due to the high coincidence of solar generation and commercial end-use loads [7, 8].

A number of studies have addressed the potential electricity savings from DC distribution systems in buildings [5, 9–26]. For the commercial sector, the reported savings differ widely, from 2% [9] to as much as 19% [10]. Higher savings were reported in systems that were connected to a DC source such as PV and batteries. In general, the reported savings are highly dependent on the converter efficiencies for the AC and DC distribution systems, the DC distributions system topology and voltage levels, and the coincidence of loads with PV generation. For example, Denkenberger, et al. [11] estimated 2% electricity savings for a typical code-compliant office building and 8% savings for a zero net energy (ZNE) office building with on-site PV generation. Sannino, et al. [12] calculated power losses in a commercial building DC distribution system for different voltage levels (48, 120, 230, and 326 V) and compared them to losses incurred by an equivalent AC distribution system at 230 V AC. It was found that, from both a technical and economic perspective, the 326 V DC system was the optimal voltage level for the DC system.

Several existing studies have employed simple analytical models that calculate annual electricity savings by using average, static values for power conversion efficiencies [9–13]. Backhaus et al [9], who followed such an approach, recommended a more detailed simulation-based study be conducted, using realistic load and generation profiles, along with power converter efficiency curves that take into account converter performance at part load conditions. Vossos et al [14] employed a spreadsheet model for a hypothetical household with onsite PV generation in several U.S. locations. They examined the effect of battery storage and load shifting, and estimated 5% electricity savings

for systems without battery storage, and 14% savings for systems with storage. This study did take into account part load converter performance but focused on the residential sector.

Other research efforts estimate savings based on experimental test setups. Most of these studies are of narrow scope, focusing on distributing DC to a limited set of end-use loads. Weiss et al [15] estimated electricity savings in a DC office test bed operating at 380 V DC, which included PV generation, electric vehicle (EV) charging, lighting, and electronic loads. That study, although experimental, also used average converter efficiency values to calculate DC distribution system savings of up to 5.5% compared to an equivalent AC system. Boeke and Wendt [16] reported 2% measured and 5% potential electricity savings from a 380 V DC distribution system with PV generation implemented in an office LED lighting test bed at the Philips High Tech Campus, in Eindhoven, Netherlands.

Few studies have used detailed, validated simulation models to estimate energy savings. Fregosi, et al. [17] employed energy analysis simulation tools to assess the performance of a high bay LED DC distribution system. The simulation software developed by the National Renewable Energy Laboratory (NREL) considered various commercial building types, operating schedules, system configurations, and climate zones to project 6%-8% electricity savings by using DC distribution. The study, although based on validated simulation models, was limited in scope and did not account for realistic converter efficiencies at part-load conditions.

This work addresses a pressing need for a more detailed simulation-based study that compares the efficiency of equivalent AC and DC building networks. The research improves on many previous works by comprehensively accounting for solar generation, storage, and the complete building load profile. In addition, it provides recommendations on how DC power systems can support the development of ZNE and islanding microgrid buildings.

This work uses highly detailed Modelica simulations to improve on previous works in the following ways:

- The simulations utilize annual data from detailed and realistic load and generation profiles.
- The building networks use real converter market data and precise wire models in order to accurately quantify the system loss.
- Parametric simulations are performed in order to determine the range of potential electricity savings with DC, and identify ways to maximize those savings.

- A loss breakdown and analysis attributes the savings and loss to specific components in the electrical distribution network.

Section 2 discusses the modeled building distribution network topologies and voltage rails. In Section 3, the paper explains the modeling assumptions for each type of component within the building model. Section 4 describes how the parametric simulations are performed. Finally in Section 5, the simulation results are presented and discussed.

2. Building Distribution Network Topologies

The building network topologies are categorized by their distribution and coupling. Distribution refers to how the building's electrical power is delivered to the loads, and designates whether the network should be considered AC or DC. Coupling refers to how the PV array is connected to the battery. Network topologies are denoted by their distribution type, along with a subscript of their coupling setup. This study examines and compares two network topologies:

- $\mathrm{AC}_{\mathrm{AC}}$: AC electrical distribution and AC PV to battery coupling
- $\mathrm{DC}_{\mathrm{DC}}$: DC electrical distribution and DC PV to battery coupling

A variety of alternate network topologies are described in Appendix B.

Simulations are performed on models of small and medium office buildings using the Department of Energy's (DOE's) Energy-Plus reference buildings for dimensions and load profiles [27–29]. These reference buildings contain detailed and realistic models based on building characteristics, codes, requirements, and regional climate data. The diagrams of each network topology are shown in Figures 2 to 5. Building size affects the building's selected distribution voltages. The simulated models utilize one or more of the following power distribution voltages:

- AC Low Voltage: 120 $\mathrm{V_{RMS}}$ single phase (208 $\mathrm{V_{RMS,L\text{-}L}}$ for three phase)
- DC Low Voltage: 48 V
- DC High Voltage: 380 V (only in medium office building)

The 48 V DC rail represents a power over ethernet (PoE) style power distribution [30–32]. The 380 V DC rail follows the EMerge Alliance 380 V DC standard for power distribution to data centers [33–35].

Each building topology in Figures 2 to 5 has several types of essential power converters. They can have one or more of the following special functions:

- *Bidirectional (BiD)*: Power can flow into either port.
- *Maximum Power Point Tracking (MPPT)*: Capable of performing the MPPT algorithm on a DC port. Can interface with a solar array.
- *Charge Controller (CC)*: Capable of controlling charge flow on a DC port via a battery charging algorithm. Can interface with a battery bank.

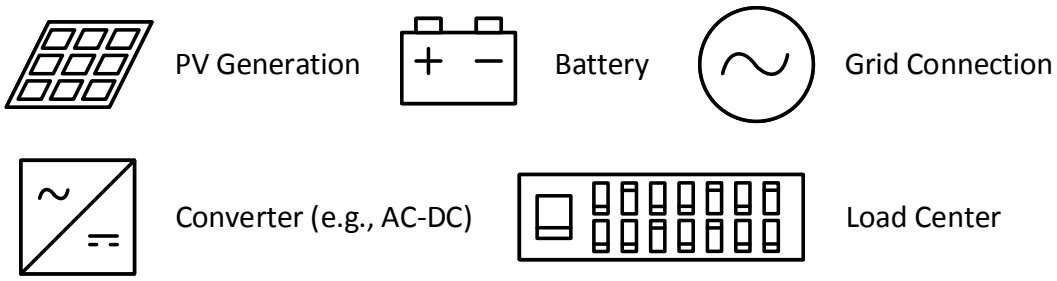

Figure 1: Symbol guide for topologies in Figures 2 to 5.

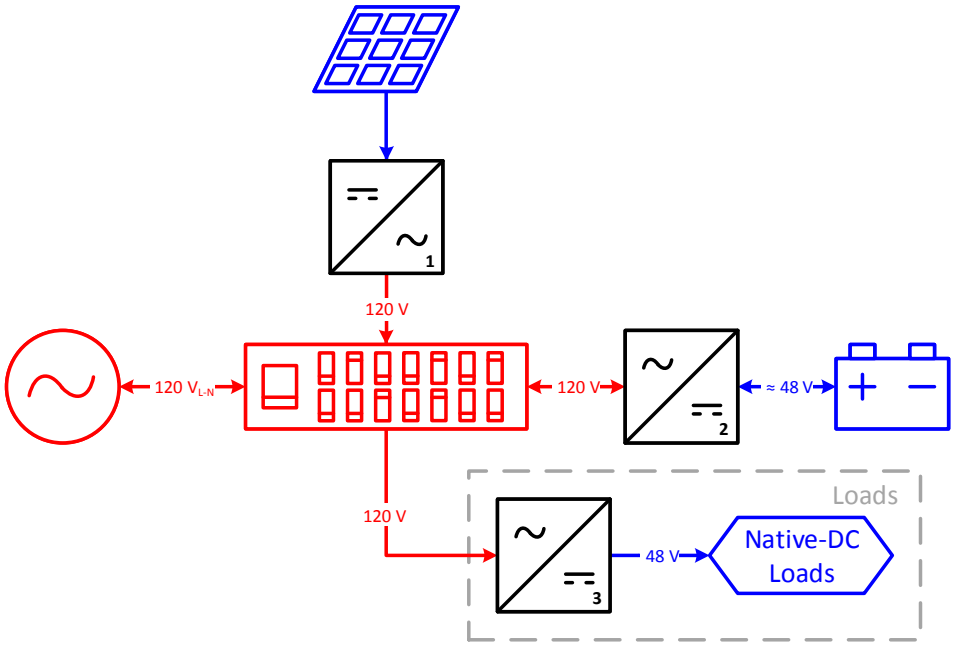

Figure 2: Small office building network AC_{AC}: AC distribution AC coupled. Converters: 1. string inverter (MPPT), 2. battery inverter (BiD, CC), 3. load-packaged rectifier.

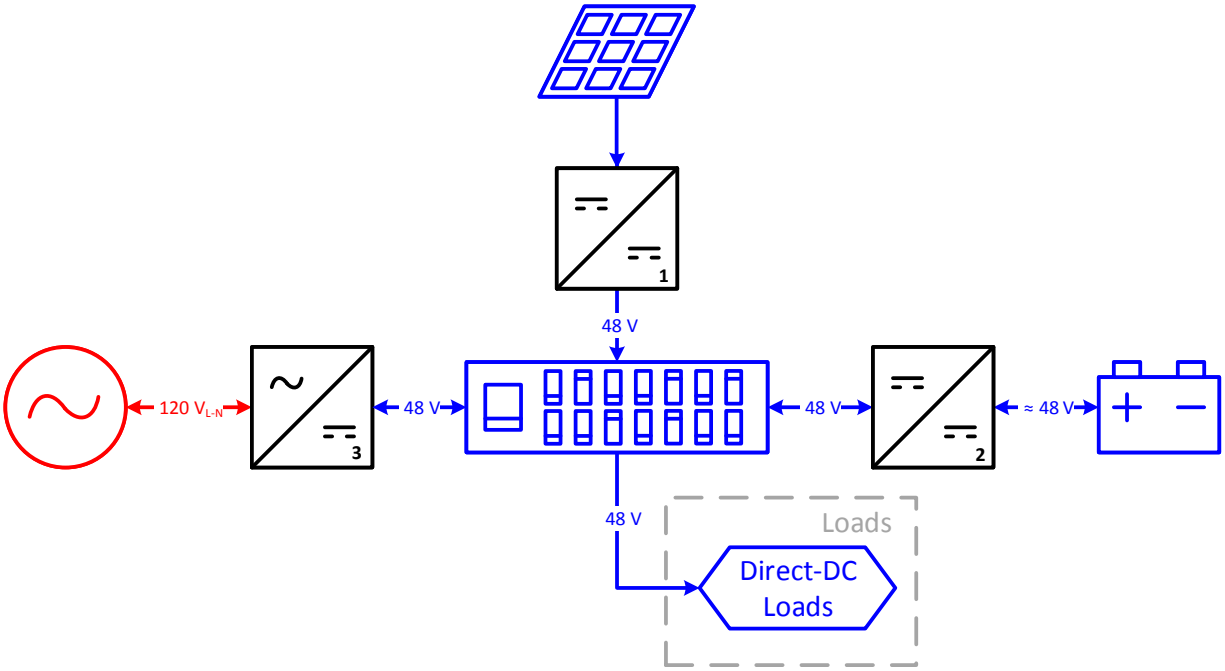

Figure 3: Small office building network DC_{DC}: DC distribution DC coupled. Converters: 1. MPPT module (MPPT), 2. battery charge controller (BiD, CC), 3. grid tie inverter (BiD). Certain loads such as LEDs require an additional DC-DC converter (not shown).

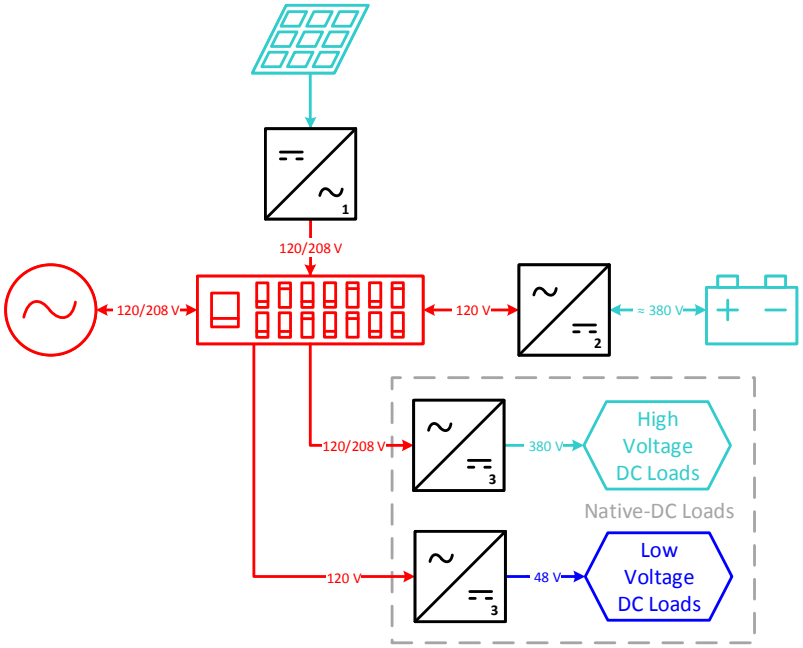

Figure 4: Medium office building network AC_{AC}: AC distribution AC coupled. Converters: 1. string inverter (MPPT), 2. battery inverter (BiD, CC), 3. load-packaged rectifier.

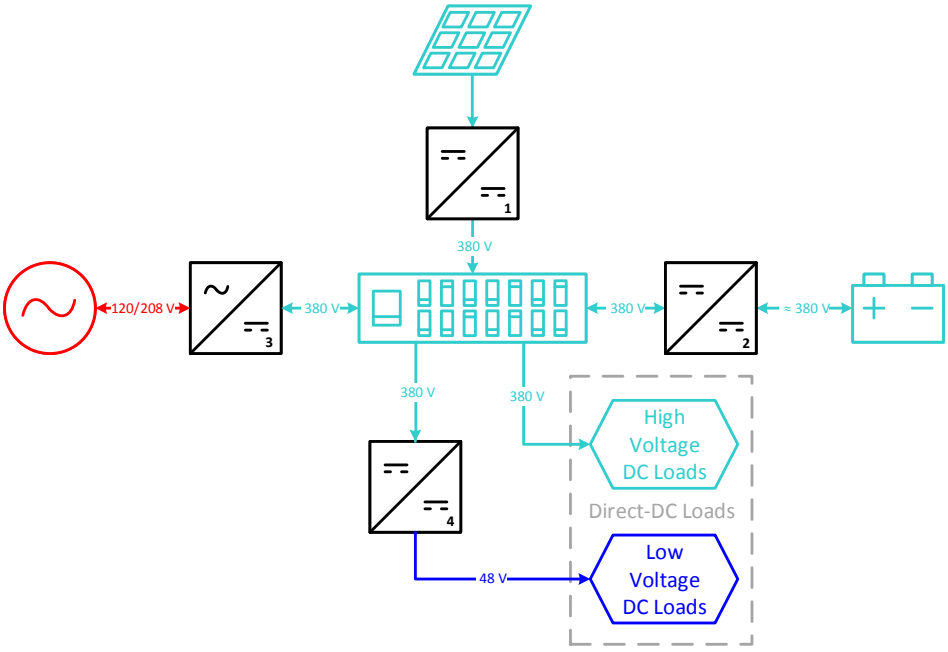

Figure 5: Medium office building network DC_{DC}: DC distribution DC coupled. Converters: 1. MPPT module (MPPT), 2. battery charge controller (BiD, CC), 3. grid tie inverter (BiD), 4. DC-DC step-down. Certain loads such as LEDs require an additional DC-DC converter (not shown).

3. Components of the Building Electrical Network

The electrical sources and sinks in the modeled building are the loads, solar generation, battery, and a grid connection. The electrical losses in the modeled building are attributed to converters, building distribution wiring, and chemical losses in the battery. This section describes the modeling setup and assumptions for the sources, sinks, and loss components in the building network model.

3.1. Load Center

The load center is a panelboard through which all of the building's loads are connected. Similar to the modeling done by Backhaus, et al. at Los Alamos National Laboratory [9], the modeled loads in this research are all assumed to be operating internally on DC. DC loads are either direct-DC or native-DC, depending on whether the building's electrical distribution network is DC or AC, respectively. Direct-DC loads may either connect directly to the DC building distribution or utilize a DC-DC converter to step the input voltage to an appropriate level. Native-DC loads always require a rectifier to interface with the AC building network.

The modeled load profile comes from a DOE reference building in Los Angeles [27–29]. Hourly electrical load data is provided for heating, cooling, fan, interior lighting, exterior lighting, and interior equipment. Appendix A.1 provides additional details on how the loads are modelled.

3.2. Solar Generation

The photovoltaic (PV) array is modeled as a time variant power source. Its output is determined by the amount and angle of solar irradiation in Los Angeles (from PVWatts) [36, 37]. The PV panels are always operating at a constant MPPT voltage, which is a reasonable approximation for most panels [38, 39]. The MPPT voltage is usually two to three times that of the distribution voltage, and is chosen based on the component data.

3.3. Converters

Converters contribute the most to overall building network electricity loss, and the DC building network is designed to reduce the number of conversions. In general, the efficiency of converter products increases with power capacity and operating voltage.

Each converter in Figures 2 to 5 has a representative efficiency curve (i.e., efficiency as a function of its output power relative to its maximum output power capacity) based on data from converters currently available on the market. Efficiency data can be obtained as visual curves from datasheets,

or as select data points from sources such as the study done by the California Energy Commission [40]. Appendix E shows the set of efficiency curves used in this study.

In order for a converter's efficiency curve to simulated, its rated power capacity must be known. At every conversion stage, the modeled building is assumed to contain enough parallel converters to meet the peak power requirements. The conversion stage power is equally distributed over all the converters at all times. Rated power capacity and operating voltage are the main factors in chosing converter product data that provides a consistent and accurate comparison between AC and DC.

Converters often have a negative impact on power quality. Line current harmonics generated at the input of rectifiers can contribute to wiring loss in the grid; however, harmonic distortion isn't very significant to the scope of this study since the AC and DC distribution networks both require an eventual rectification stage. In addition, many converters have power-factor correction front-end circuits that greatly reduce input current harmonics. Switching rectifiers and inverters often have a displacement power factor greater than 0.99 and total harmonic distortion less than 5% [9]. As such, harmonic distortion is considered to have a second-order impact on building efficiency and is not modeled. It is important to note that many AC loads currently on the market do not use switching rectifiers and have a considerably lower power quality (for example, induction motors or low power wall adapters). Because power quality can be important for other reasons, in-depth power quality simulations are encouraged in future work.

3.4. Battery

The battery operates as a source or sink, when discharging or charging, respectively. There are many types of batteries, each of which is well suited for certain climates and techno-economic conditions. In this work, a representative generic battery is modeled, since the type of battery is less significant in a comparison of AC and DC distribution.

To ensure safety and longevity, batteries require a charge controller. The controller prevents battery damage and degradation by enforcing a maximum charge or discharge current and limiting the depth of discharge. The modeled battery controller in this work uses a simple charging algorithm, similar to the work done by Hittinger, et al. 2015 [41]. The controller charges the battery when the PV output power exceeds the load demand. Likewise, it discharges the battery when the load exceed the PV. As such, grid export or import is only allowed when the battery is fully

charged or discharged, respectively. Appendix A.2 discusses the battery controller in detail.

In practice, many battery controllers contain complex charging schedules. Battery controllers may employ multi-stage charging or equalization schedules so as to maximize the battery life span. They may also be configured to charge from the grid when the import tariff is low. The battery controller in this work does not account for either of these features in its charging algorithm. Multi-stage charging and equalization are largely second-order effects in comparing AC to DC. Tariff-based grid import is not considered because this work assumes a future scenerio in which charging the battery from solar generation will always be more economic than grid import.

The modeled battery voltage is set to a constant 48 V or 380 V, which is chosen to reflect product data for both AC and DC. Nonetheless, it is useful to note that battery converters can have higher efficiency when the battery voltage is matched to the distribution voltage. In practice, the battery voltage is correlated with its SOC. However, the battery model in this work approximates the battery voltage as constant since variations in battery voltage are relatively small. Nonetheless, the battery voltage affects the converter and chemical loss, and precise battery models are encouraged in future work.

3.5. Building Wiring

Wiring loss can be substantial in larger buildings with low distribution voltage. As such, it is common for larger buildings to be designed with a high voltage backbone and a low voltage local distribution.

Since the wiring loss is due entirely to resistive I^2R losses (skin effect and inductive losses are ignored), the building's wires are modeled as resistors. The resistance of a wire is calculated from its length and resistance per length (Ω/m). The length is determined and modeled via geometric methods. The Ω/m is based on the ampacity of the modeled loads. The exact procedure for modeling the wires is explained in Appendix A.3.

This study does not account for losses in protective equipment such as the breakers in a panelboard. These losses are relatively small in 20 A rated breakers, and become even less significant at higher ampacity.

4. Modelica Simulation Procedure

The main purpose of simulation is to compare the efficiency of equivalent AC and DC building distribution networks. It is also desirable to determine the most suitable conditions for a DC

network. Parametric simulations are necessary to accomplish these goals. All of the simulations except those described in Appendix D have a year-long simulation duration. This section describes the procedure for selecting parameters and performing simulations.

4.1. Simulation Parameters

The parametric simulations are organized into experiments. In each experiment, several inputs are parametrically varied in order to test for a specific result. For each parameter, a baseline value is established as an experimental control. The following parameters can be selected as parametric inputs:

- *Solar capacity*: The maximum output of the solar array in the best conditions. The baseline value is the solar capacity required for a ZNE building.
- *Battery capacity*: The storage capacity of the battery. The baseline value is 50% of the battery capacity required for the ZNE building to store all excess solar on the sunniest day.
- *Converter oversize ratio*: How much the converters are oversized relative to their peak power. The baseline value is 150%, which is a typical case.
- *Converter efficiency curve*: Specifies whether converters should use the median or maximum of efficiency curve sets. The baseline is the median efficiency curve, which is a typical case.
- *Starting day*: The day of year to start simulation, which affects PV generation and load profiles. Only relevant for simulations in Appendix D.

The baseline value for the solar capacity is found by determining the required solar capacity such that the annual solar generation energy matches the annual load energy. As mentioned in Section 3, the annual hourly solar and load profiles are obtained from PVWatts and the DOE reference buildings respectively.

Many published works detail theoretical methods for sizing the battery for either stand-alone or grid-connected systems [42–46]. Most of these methods solve an intricate convex optimization problem. Economically sizing the battery for grid-connected networks also requires knowledge of the hourly electricity tariff. In this work, the battery controller described in Section 3.4 is designed to minimize grid intake, and thus ignores electricity rates. In addition, the availability of hourly PV and load data allows for most of the equations in [42–46] to be simplified or ignored.

The baseline value for the battery capacity is found by measuring the daily excess solar energy. The daily excess solar energy E_{solar}^{excess} can be determined from:

$$P_{solar}^{excess} = P_{solar} - P_{load} \quad (1)$$

$$E_{solar}^{excess} = \int_{day} (P_{solar}^{excess} | P_{solar}^{excess} > 0) \quad (2)$$

where P_{solar} is the total solar generation power, P_{load} is the total load demand, and P_{solar}^{excess} is the hourly excess solar power. The largest the battery should ever be sized, C_{max}, is the maximum value of E_{solar}^{excess} over a full year. Sizing $C > C_{max}$ adds unutilized capacity. Batteries are expensive, and smaller batteries are often desirable in grid-connected buildings. As such, the baseline battery capacity is established as 50% of C_{max}. For the PV conditions in Los Angeles, this baseline value can successfully store E_{solar}^{excess} for roughly 75% of the days. Battery capacities at or above the baseline value may be relevant for islanding microgrid buildings.

4.2. Simulation Software Flow

The AC and DC building networks are modeled in Modelica. The use of Modelica has become prevalent in buildings research because it allows for precise customized transient simulations. In

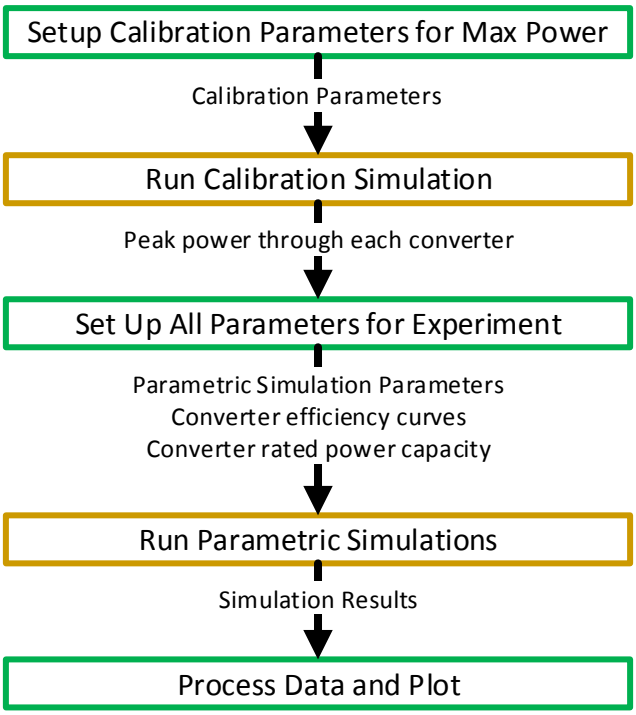

Figure 6: Simulation flow block diagram. Python processes are boxed in green, and Modelica processes are in yellow.

addition, Modelica can model combined electrical and mechanical systems, which may be useful in future work.

The parametric simulations are managed in Python. In each parametric run, Python opens an instance of Modelica and passes the necessary parameter values. The actual transient simulations for the building distribution network are executed in Modelica via Dymola. The Modelica model contains all connections and equations defining each of the distribution networks for each building. After the transient simulations are complete, Python can interpret and plot the results.

The complete simulation flow is depicted in Figure 6. An initial calibration simulation must be performed before each parametric simulation. The purpose of the calibration step is to automatically size the converters by determining the yearly maximum amount of power each converter must handle. This is a conservative maximum, and so the calibration simulation sets the efficiency of each converter to its peak efficiency curve value.

5. Results and Discussion

5.1. Overview of Experiments

Simulations are performed on the modeled small and medium office buildings. For each building, the efficiencies of the $\mathrm{AC_{AC}}$ and $\mathrm{DC_{DC}}$ topologies are compared. Building network efficiency is calculated as:

$$\text{Efficiency} = 100(1 - \frac{E_{Loss}}{E_{Load}}) \tag{3}$$

where E_{Loss} and E_{Load} are the total annual loss and load energy, respectively.

For each modeled building, three parametric experiments are performed in order to determine when DC is most advantageous. The solar and battery experiments observe the effect of varying the solar capacity and battery capacity, respectively. The converter experiment observes the effect of varying the quality and size of the converters used in the building.

It is important to note that the parameter values are selected to simulate a wide range of scenarios. Many of these scenarios are not necessary or practical at present, but could easily be considered in the future as renewables become prevalent. For example, the ZNE baseline is an important scenario because the California Public Utilities Commission has plans to achieve ZNE in residential buildings by 2020 and commercial buildings by 2030 [47–50].

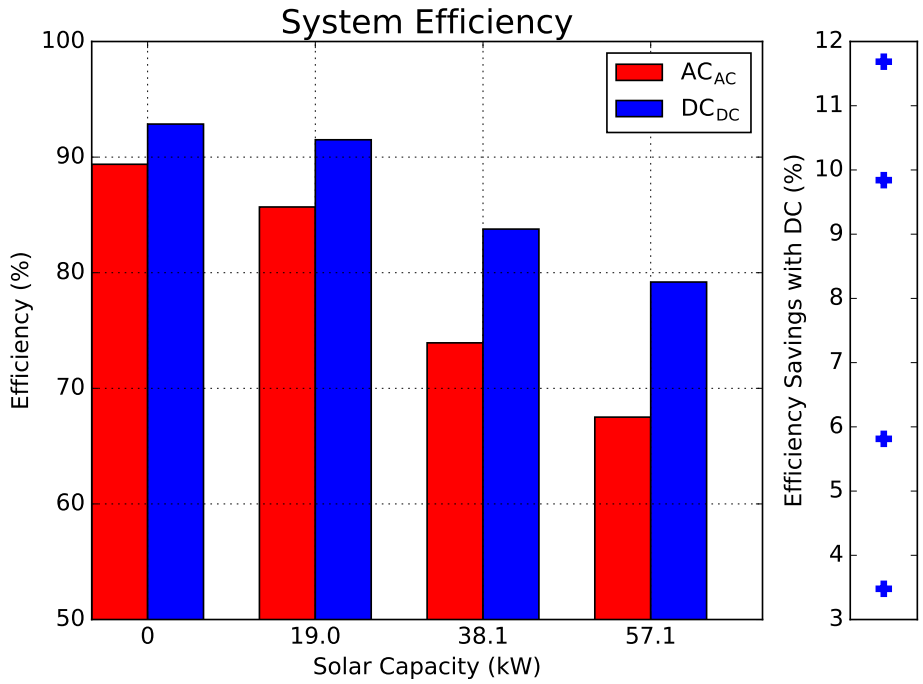

(a)

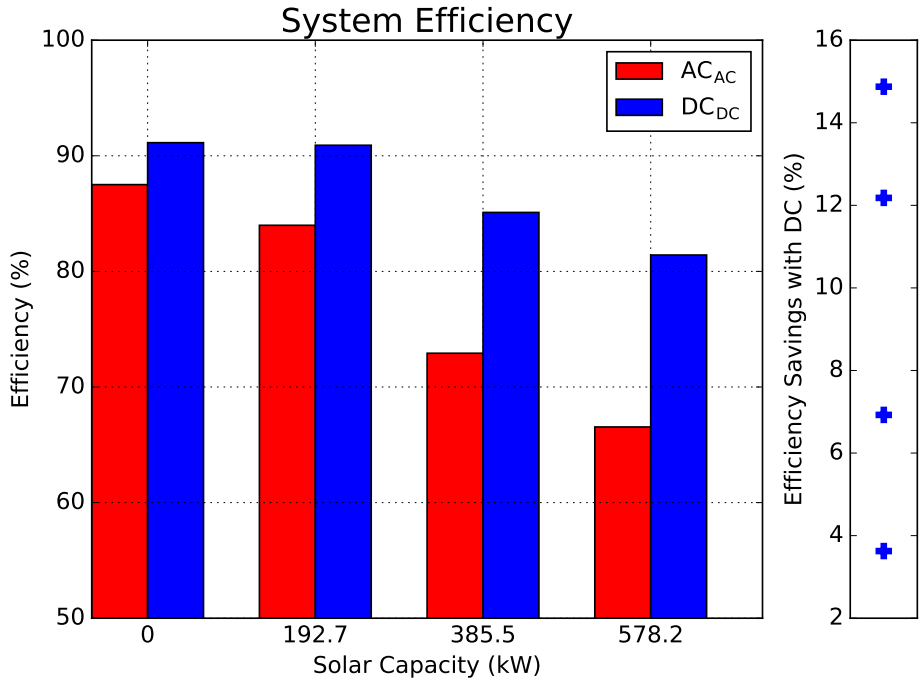

(b)

Figure 7: The solar experiment for (a) the small office building, and (b) the medium office building. This experiment observes the effect of setting the solar capacity parameter to 0%, 50%, 100%, and 150% of the baseline value. The baseline is the solar capacity required for a ZNE building. 150% of the baseline represents a building that is designed as a power producer. As a control, the battery is also scaled by the same percentages relative to its baseline. For reference, the roof area can hold up to 81.67 kW in the small building and 266.4 kW in the medium (not including parking canopies, etc).

5.2. Solar Experiment

As shown in Figure 7, the efficiency savings with DC distribution increases with solar capacity. However, the savings begins to level off as the solar capacity is increased past the ZNE baseline. DC distribution is optimal when use of the grid tie inverter is minimized. Whenever the building must engage in grid import or export, the grid tie inverter incurs a substantial loss. Frequent grid export can happen because of an oversized solar capacity or an undersized battery.

In buildings with a small solar capacity, most of the load demand is supplied from the grid. The rectification stage occurs at the grid tie inverter for DC_{DC}, and the load-packaged rectifiers for AC_{AC}. Grid tie inverters are optimized for high power, and generally have higher efficiency. However, the grid tie inverter is often operating at a low region of its efficiency curve. In addition, certain direct-DC loads such as LEDs require an additional driver, thus presenting two conversion stages between the grid and load. For these reasons, DC distribution provides very little benefit in buildings with small solar capacity.

5.3. Battery Experiment

As shown in Figure 8, the DC_{DC} topology greatly outperforms AC_{AC} as long as there is ample storage. A large battery capacity allows for minimizing the use of the grid tie inverter. In the absence of storage, a DC building should be designed with a smaller solar capacity that is matched with the load demand. Alternatively, it could contain an extra MPPT inverter to export excess solar directly to the grid.

The grid tie inverter in DC_{DC} will always have some use even if the battery is drastically oversized. Seasonal effects make it impossible to size the solar capacity to perfectly match the load demand. Even at 200% of the baseline capacity, there is still some grid import during the winter and grid export during the summer.

5.4. Converter Experiment

The results shown in Figure 9 reveal that the efficiency of DC products has a smaller spread than for AC products. The reason is that the efficiency of DC products is already nearly 100%, as shown in Appendix E. In some sense, the maximum efficiency curves represent the average quality of products in the future. As such, AC products have much more room for improvement than DC products.

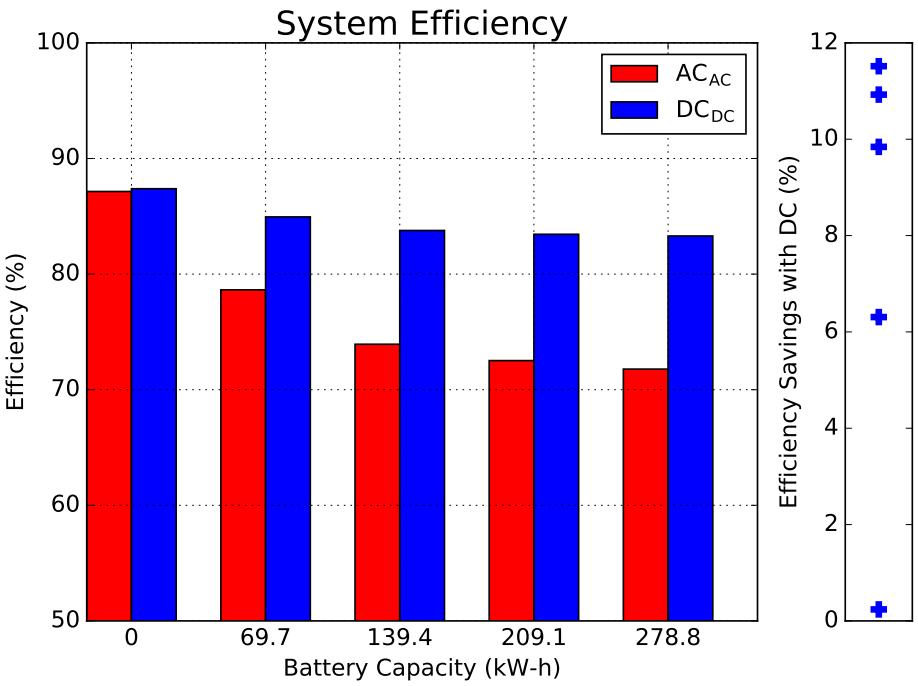

(a)

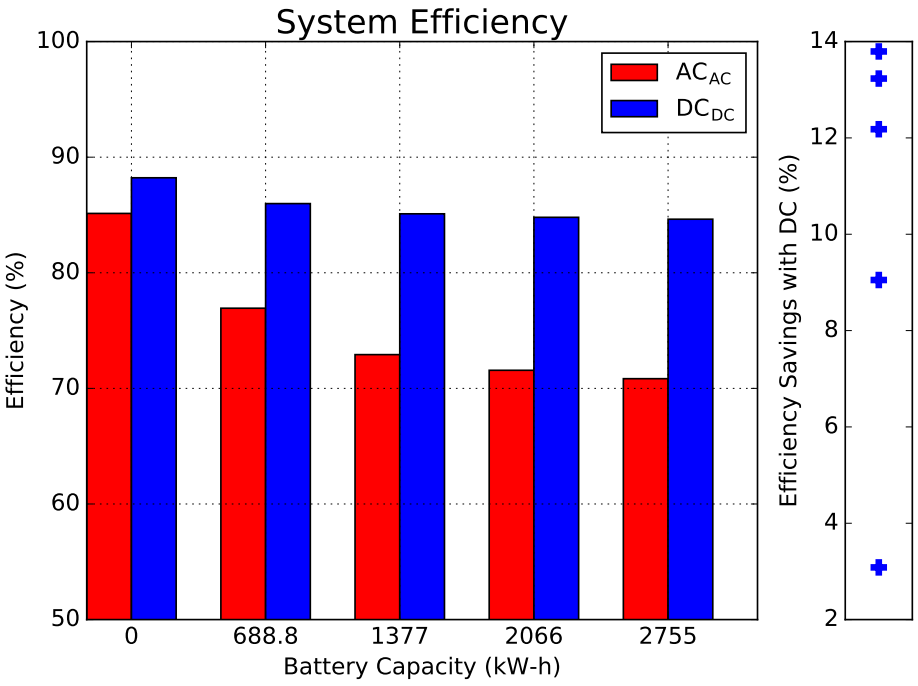

(b)

Figure 8: The battery experiment for (a) the small office building, and (b) the medium office building. This experiment observes the effect of setting the battery capacity parameter to 0%, 50%, 100%, 150%, and 200% of the baseline value. The baseline is 50% of the smallest size required to store the excess solar on the sunniest day.

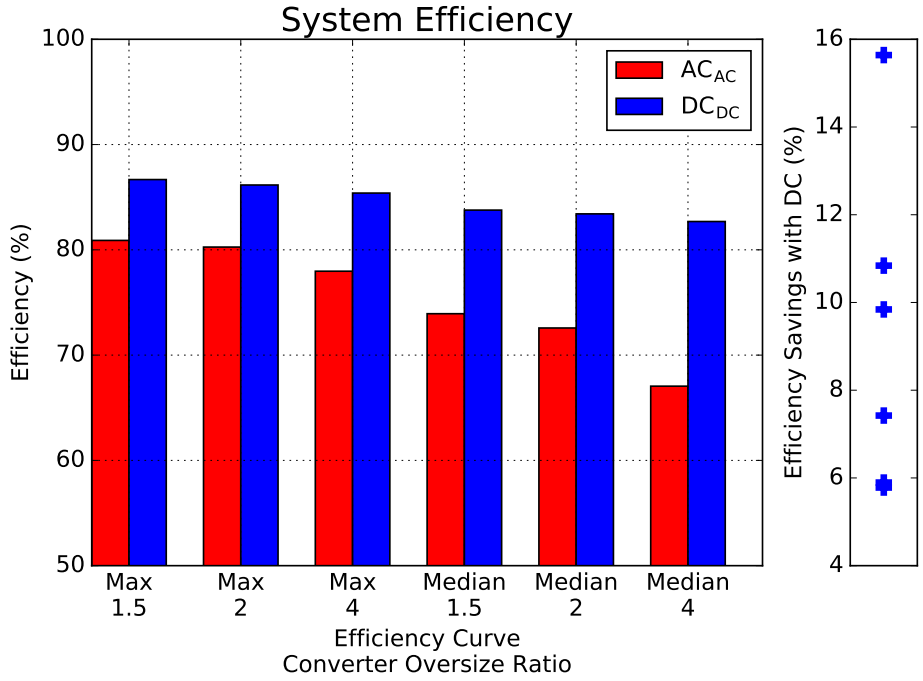

(a)

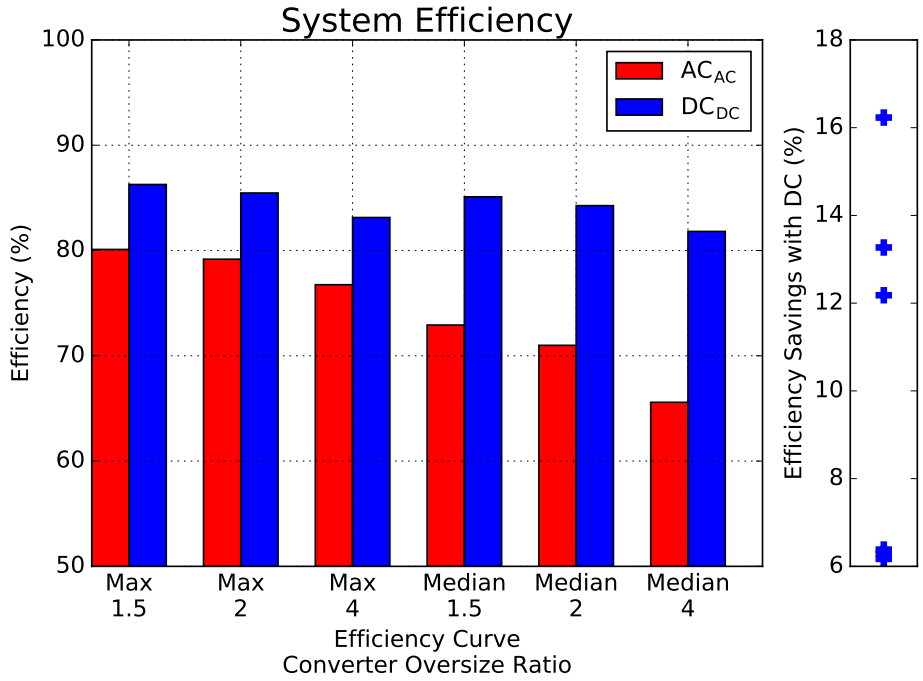

(b)

Figure 9: The converter experiment for (a) the small office building, and (b) the medium office building. This experiment observes the effect of the quality and size of the converters used in the building. In this experiment, the converters all use either the median or maximum efficiency curves, and have oversize ratios of 150%, 200%, and 400%.

	Baseline parameters	Best-case scenario
Small office building	9.9%	17.9%
Medium office building	11.9%	18.5%

Table 1: Percent efficiency savings with DC for baseline and best-case parameters in a small and medium office building.

The converter experiments also reveal how the relative efficiencies of AC and DC products change with their oversize ratio. The converter oversize ratio translates to the converter's operating region on its efficiency curve. The results in Figure 9 show that AC products generally perform substantially worse when operating at low power. In practice, designers will never oversize converters by 400%. However, the 400% oversize ratio can be somewhat representative of a building operating at half its population capacity.

5.5. Baseline and Best-case Savings with DC

For both buildings, $\mathrm{DC_{DC}}$ outperforms $\mathrm{AC_{AC}}$ in nearly every experiment. The efficiency savings with DC is summarized in Table 1. The best-case scenario represents an upper bound on efficiency savings, in which all of the parametric values are unrealistically advantageous for DC. Specifically, this means that the solar capacity is 150% of baseline, the battery capacity is 200% baseline, and the converter oversize ratio is 400%.

In addition to the small and medium buildings, a large office building is simulated. As explained in Appendix C, the baseline efficiency savings is only 7.5% in the large building. This is primarily due to the 480 $\mathrm{V_{RMS,L\text{-}L}}$ backbone in the $\mathrm{AC_{AC}}$ large office building that greatly improves conversion efficiency and decreases wiring loss.

5.6. Loss Analysis

The loss breakdown for the small and medium buildings is shown in Figure 10. The percent loss of component n is calculated as:

$$\text{Percent Loss} = 100\left(\frac{E_{Loss,n}}{E_{Load}}\right) \tag{4}$$

where $E_{Loss,n}$ is the annual loss energy of a specified component, and E_{Load} is the total annual load demand.

In this analysis, the solar capacity and battery size are parametrically varied. The results lead to several immediately apparent observations. First, load-packaged rectifiers cause the most

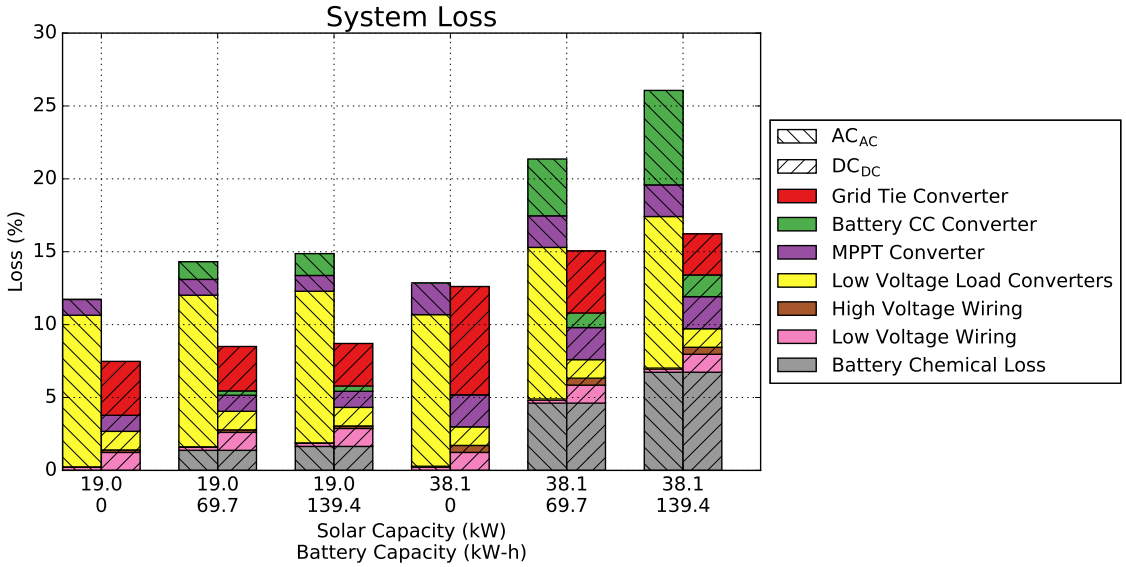

(a)

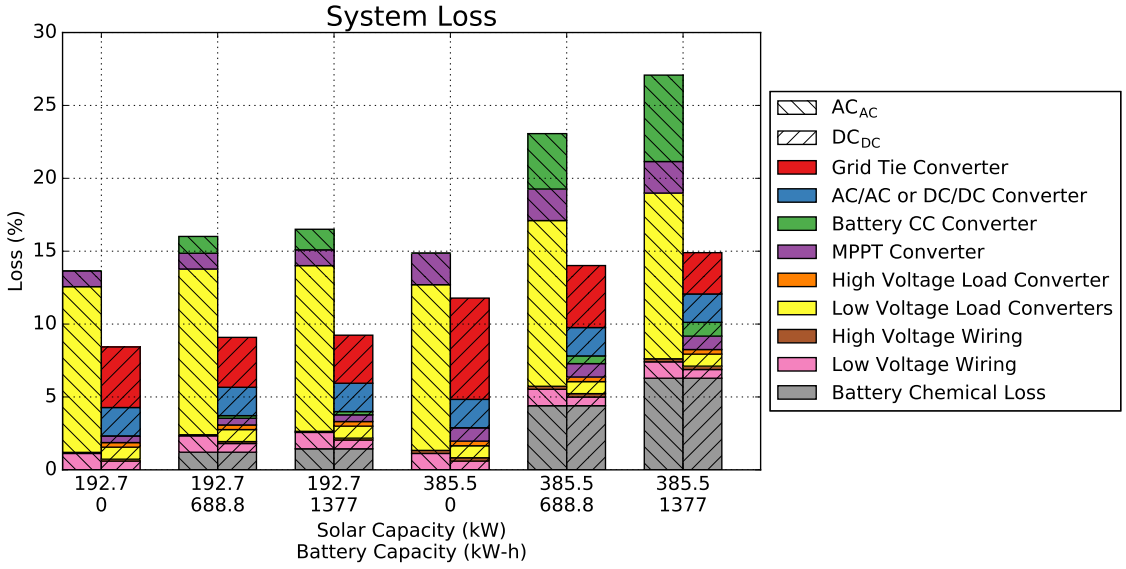

(b)

Figure 10: Loss analysis for (a) the small office building, and (b) the medium office building. Solar capacity is 50% and 100% of the baseline. Battery capacity is 0%, 50%, and 100% of the baseline. Converters are categorized by function. Battery CC converters include battery inverters and DC-DC charge controllers. MPPT converters include string inverters and MPPT DC-DC modules. Load converters include any of the load-packaged rectifiers and DC-DC LED drivers. In all buildings, the solar panel wiring is categorized as high voltage.

loss in the AC_{AC} topology. As shown in Figure E.21, load-packaged rectifiers are not optimized for high power and are relatively inefficient. Second, the grid tie converter loss is very high in batteryless DC_{DC} buildings with a large solar capacity. The fourth pair of bars in Figure 10 shows that a batteryless ZNE building barely benefits from DC distribution. Finally, the use of a battery

introduces a considerable amount of loss in both grids, particularly for the ZNE baseline solar capacity. The practicality of storage in a grid-connected system is debatable and generally varies by region. However, if a battery is to be introduced, it is important to note that DC-DC battery charge controllers greatly outperform AC battery inverters.

The loss breakdown also reveals some fundamental differences between the DC_{DC} topologies for the small and medium office buildings. First, the 380 V MPPT converters and battery charge controllers perform significantly better than their 48 V counterparts. The trade-off is that a 380 V to 48 V DC-DC converter is necessary to deliver power to the low voltage loads in the medium building. Second, the unusually low 48 V distribution causes the small office building to have considerably more wiring loss.

6. Conclusion

This work aims to assist and inform an industry decision on whether to use DC power distribution in buildings. In contrast to previous research, this work uses highly detailed Modelica simulations to compare equivalent AC and DC building distribution networks with generation and storage. The electrical building models are composed of realistic load and generation profiles, converter efficiency curves based on market data, and precise wiring models. The results of this study are useful in guiding the design and development of ZNE and islanding microgrid buildings.

Parametric simulations are performed with baseline values that correspond to a ZNE building with a generous battery capacity and properly sized converters. This research found that the baseline efficiency savings of a small and medium office building with DC distribution are 9.9% and 11.9%, respectively. The best case scenario yields savings of 17.9% and 18.5%. This study also confirms that DC distribution is best suited for buildings with a large solar capacity, a large battery bank, and a high voltage distribution backbone.

The experimental results contain many scenarios that are not necessarily practical or representative of current designs, but are interesting and important from a visionary perspective. The solar capacity baseline is important because ZNE buildings will likely become prevalent in the next two decades [27–29]. The battery experiments are harder to justify since the introduction of storage incurs a great cost in both economics and efficiency. Nonetheless, as on-site renewable generation becomes prevalent, the grid export tariff may become significantly lower than that of grid import [51]. Eventually, on-site storage may be of great value to grid-connected buildings. In addition,

large battery capacity is crucial for islanding microgrid buildings.

Although this work contributes in establishing a baseline for efficiency savings with DC, other metrics besides efficiency must be examined in order to reach a decisive verdict. For example, this study does not account for power quality. While power quality may translate to efficiency loss in the grid, there are other important ways in which a system can suffer from low power quality. Ultimately, a comprehensive techno-economic analysis is required to thoroughly measure the savings of DC distribution. Such an analysis would ideally encompass the differences in up-front cost, life-cycle cost, metering (i.e., efficiency), and power quality.

7. Acknowledgements

This work was supported by the Assistant Secretary for Energy Efficiency and Renewable Energy, Building Technologies Office and the U.S. China Clean Energy Research Center, Building Energy Efficiency (CERC-BEE) program, of the U.S. Department of Energy under Contract No. DE-AC02-05CH11231.

The authors would like to thank Luna Schector, Aditya Khandekar, Mattia Pezzola, and Nirali Merchant for their technical advice and expertise. Additional thanks to Seth Sanders for graduate advising and support. Special thanks to Kyra Epstein and the other editors and reviewers for their constructive feedback on improving the manuscript.

Appendix A. Detailed Description for Building Component Models

Appendix A.1. Load Center

The heating, ventilation, and air conditioning (HVAC) is modeled as a set of 24-Amp packaged rooftop variable refrigerant flow (VRF) units. These VRF units represent the load profile for cooling, heating, and fans [27–29], each of which are modeled as variable frequency drive (VFD) motors in the VRF compressor. VFDs contain an internal DC stage and an inverter that powers the stator coils [9]. It is assumed that future VFDs designed specifically for direct-DC will be able to connect directly to the DC distribution lines, and do not require an input DC-DC converter.

The interior and exterior lighting is modeled exclusively as LED lamps. LEDs require precise current regulation, and therefore cannot be connected directly to the DC distribution lines. As such, the modeled lamps require either an AC or a DC LED driver to interface with the distribution.

The modeled lamps do not utilize dimming, and thus operate at a constant 75% maximum power when turned on.

The interior equipment load profile is mostly from office electronics. In 2012, Cisco introduced methods for a 60 W variant of 48 V PoE on a 802.3at cable [30–32], which is enough power to charge most small laptops and tablets. The modeled interior equipment is 48 V PoE capable and can connect directly to the DC distribution without a DC-DC converter. Computers contain an internal power supply with several DC-DC converters that step-down the input voltage to the various internal voltage rails. This power supply is required for both direct-DC and native-DC computers, but the native-DC computer also requires a rectifier.

Appendix A.2. Battery Controller

The battery controller uses a simple algorithm that depends solely on the excess solar power P_{solar}^{excess}, defined in Equation 1. The controller attempts to charge the battery when $P_{solar}^{excess} > 0$, and discharge when $P_{solar}^{excess} < 0$. As such, the battery controller requires real-time information about the total solar output and load demand. The transient plots in Appendix D show how the battery controller follows P_{solar}^{excess}.

The battery may charge up to a maximum state of charge (SOC) of 100%; however, it may only discharge to a 25% SOC to preserve the integrity and life span of the battery unit. This lower limit is determined as the average of the minimum SOC for a lead-acid battery with a 1000-2000 cycle life span, and a lithium-ion battery with a 3000 cycle life span [52–54].

The simulation model also specifies the maximum rate of charging and discharging. In Jin, et al. 2007 [55], the maximum charging and discharging power is

$$P_{max}^{chg} = C(1 - SOC)\tau_{chg} \quad \text{(A.1)}$$

$$P_{max}^{dis} = C(SOC)\tau_{dis} \quad \text{(A.2)}$$

where C is the rated battery capacity and τ is a constant that adjusts the charge and discharge rates.

In practice, battery datasheets usually contain values for the absolute maximum rated charge and discharge power, $P_{max,rated}$. In this study, $P_{max,rated} = C/4$ as was done in Hittinger, et al. 2015 [41]. For this model, τ can be derived from $P_{max,rated}$ for $SOC_{max} = 100\%$ and $SOC_{min} = 25\%$.

$$
\begin{aligned}
P^{chg}_{max,rated} &= C(1 - SOC_{min})\tau_{chg} = C/4 \\
\tau_{chg} &= \frac{P^{chg}_{max,rated}}{C(1 - SOC_{min})} = \frac{1}{3} \qquad \text{(A.3)} \\
P^{dis}_{max,rated} &= C(SOC_{max})\tau_{dis} = C/4 \\
\tau_{dis} &= \frac{P^{dis}_{max,rated}}{C(SOC_{max})} = \frac{1}{4} \qquad \text{(A.4)}
\end{aligned}
$$

The battery model includes two types of chemical losses. First, energy is lost in charging and discharging the battery. The simulated model uses a charging and discharging efficiency of 90% (81% round trip), similar to the models in Jin, et al. 2007 [55] and Hittinger, et al. 2015 [41]. The other type of chemical loss is the battery's standing loss. The standing loss causes the battery's SOC to slowly decrease with time.

In Jin, et al. 2007 [55], the standing loss is modeled with a discrete time equation. For compatability with Modelica, this work derives a continuous time equivalent:

$$
\frac{d}{dt}SOC(t) = \frac{-SOC(t)\tau_{SL}}{T} \qquad \text{(A.5)}
$$

where the standing loss coefficient τ_{SL} is 0.001, and T is 3600 seconds.

Appendix A.3. Wire Resistance

Wire resistance is determined from the wire's length and its resistance per length (Ω/m). The Ω/m is referenced from the National Electrical Codes (NEC) for stranded uncoated copper wire in an aluminum conduit [56]. The wires are sized to handle 125% of the rated ampacity of their end use at 30°C ambient temperature. As per NEC guidelines, the minimum wire size is 12 AWG regardless of peak current. Since 12 AWG is larger than the loads require, it is generally safe to ignore any conduit effects on rated ampacity. Table A.2 shows the wire gauge and Ω/m for each end use.

The models require several assumptions regarding wire sizing. First, the sizing does not account for voltage drop across the wire. Second, the wires are sized for AC building distribution. This establishes the wire size as an experimental control, and allows the distribution voltage difference to be properly reflected as wire loss. Finally, the wires can combine linearly. In other words, if N wires with K Ω/m combine at a junction box, the feeder to the junction box will have N*K

Wiring End Use	Spatial Distribution	Unit Spacing	Wire Gauge	DC Ω/km	AC Ω/km
Solar panel clusters	Area	4 m	#12	6.50	6.6
Interior lighting	Area	3 m	#12	6.50	6.6
Exterior lighting	Perimeter	11 m	#12	6.50	6.6
Interior equipment	Area	3 m	#12	6.50	6.6
HVAC VRF unit (cooling, heating, fans)	Area	13 m	#10	4.07	3.9

Table A.2: Wiring for the small and medium office building. Resistance values from [56]. Solar panels are 2x1 m and arranged in 4x4 m clusters of 8 panels. For longer strings, wire gauge is assumed to combine linearly. Unit spacing for loads is based on commercial buildings of similar scope.

Ω/m. The relationship between Ω/m and rated ampacity is nearly linear between 12 AWG and 1/0 AWG, and is sufficient for the scope of this study.

The wire length is determined via geometric methods. Several additional assumptions are required for deriving the wire length model. First, the model assumes that the building's electrical room is located on the ground floor. Second, this model requires that the wires in the building are organized such that they can only traverse in the cardinal directions. In other words, wires may not traverse diagonally to the spatial X-Y axes of the building. Finally, it must be assumed that load power P_L is the same in every load unit of a given load class. In other words, $P_{L,tot} = P_L N$ for N loads.

The wiring distance d_w is defined as the distance between two points on a floor given the constraints on the wire path. For any load unit located at (x, y), the wiring distance from the load unit to the electrical room located at (x_0, y_0) can be represented as

$$d_w = |x - x_0| + |y - y_0|. \tag{A.6}$$

Given the location (x_0, y_0) and the building dimensions, the average wiring distance $d_{w,avg}$ can be determined via calculus or arithmetic methods. In addition, $d_{w,avg}$ does not depend on the modeled spatial distribution (area vs. perimeter) of the loads. For a specific wire gauge and material, the average wire resistance R_{avg} can be found from $d_{w,avg} + h_{w,avg}$, where $h_{w,avg}$ is the multi-floor height adjustment.

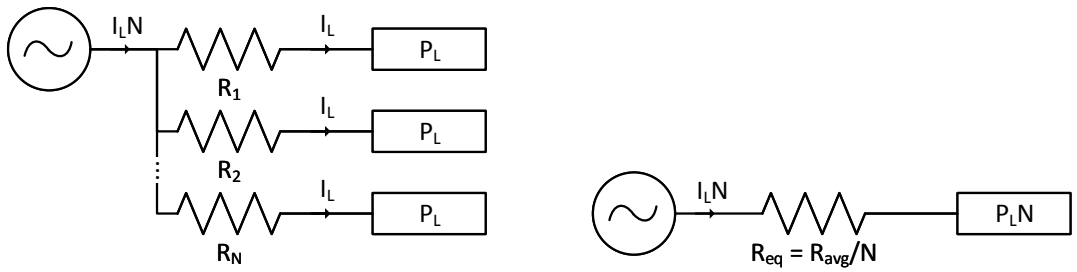

(a) (b)

Figure A.11: Distribution network wiring resistance model. (a) Model with multiple load units that are each connected to the distribution panel through a different wiring resistance. (b) Model with single power sink and lumped wire resistance.

The power lost in a wire with resistance R is $P_W = I^2R$ (for AC, assume unity power factor). In practice, I depends on the load characteristics and the wire resistance R. However, the voltage drop across the wire is assumed to be relatively small, so the voltage at the load is approximately equal to the source voltage V. With this approximation, the load voltage is decoupled from R, and the wire current I only depends on the load power P_L. As such, $I = P_L/V = I_L$, and $P_W = I_L^2R$ is now a linear function of R. This allows for superposition, and the total wire loss $P_{W,tot}$ can be developed from:

$$\begin{aligned} R_{avg} &= \frac{\sum_n R_n}{N} \\ P_{W,tot} &= \sum_n I_n^2 R_n \approx I_L^2 \sum_n R_n = I_L^2 N R_{avg} \end{aligned} \tag{A.7}$$

where N is the number of load units. Also recall that this model assumes that each load has the same P_L, I_L, and V_L.

The DOE reference building only provides Energy Plus load profile data for the total load consumption $P_{L,tot} = P_L N$ of each class of load. Modelling each individual load and wire would result in a slow and computationally intensive simulation. It is equally accurate to instead determine an equivalent lumped wire resistance R_{eq} for each load class that represents the resistance of all the wires. As shown in Figure A.11b, the entire load network can be simulated as a single resistor R_{eq} and a single power sink $P_L N$. The total current in the load network is $I_L N$, and the results from

Equation A.7 can be used to show:

$$\begin{aligned} P_{W,tot} &= (I_L N)^2 R_{eq} \\ R_{eq} &= \frac{R_{avg}}{N}. \end{aligned} \tag{A.8}$$

Appendix B. Alternate Building Network Topologies

The building network topologies in this study are categorized by their distribution, coupling, and MPPT implementation. Section 2 explains distribution and coupling. The solar MPPT implementation can be either unified or partitioned, depending on whether the solar panels are connected to a single converter or multiple micro-converters. The AC_{AC} and DC_{DC} topologies from Section 2 are both implemented with unified MPPT. The alternative topologies presented in this section are:

- AC_{DC}: AC distribution, DC coupling, unified MPPT.
- AC_{AC}': AC distribution, AC coupling, partitioned MPPT.
- AC_{DC}': AC distribution, DC coupling, partitioned MPPT.
- DC_{DC}': DC distribution, DC coupling, partitioned MPPT.

These topologies are usually only present in residences and small buildings. Diagrams for the small office building alternative topologies are shown in Figures B.12 to B.15.

The simulation results for all the small office network topologies are shown in Figure B.16. In every case, the standard AC_{AC} topology (Figure B.13) performs better than the alternative AC_{DC} (Figure B.14). The peak load demand in an office building coincides with the peak solar generation. It is therefore most efficient for the solar output to flow directly to the loads, as with AC_{AC}. DC coupled systems like AC_{DC} are generally best for buildings in which the peak load demand is out of phase with the peak solar generation [57]. In a residence, it is usually ideal for the solar output to charge the battery.

The partitioned MPPT topologies all have lower efficiencies than their unified MPPT counterparts. For AC_{AC}', this is not surprising because microinverters are generally less efficient than string inverters, as shown in Figure E.20. However, power optimizers ($AC_{DC}'$and DC_{DC}') tend to be extremely efficient. Partitioned MPPT topologies mainly suffer from excessive wiring loss. In

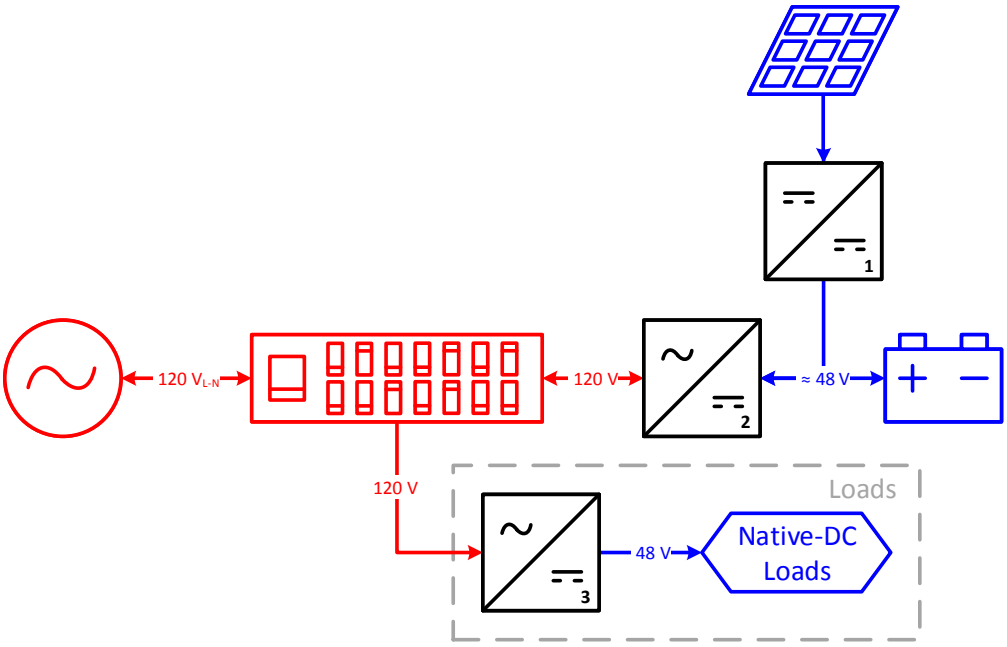

Figure B.12: Small office building network AC_{DC}: AC distribution DC coupled with unified MPPT. Converters: 1. MPPT charge controller (MPPT, CC), 2. battery inverter (BiD, CC), 3. load-packaged rectifier.

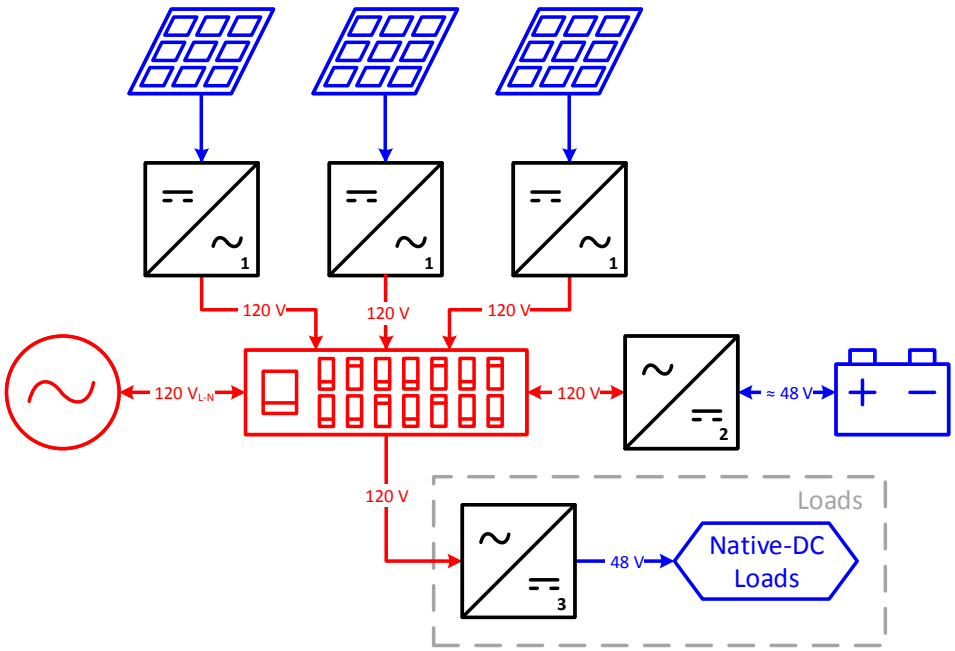

Figure B.13: Small office building network AC_{AC}': AC distribution AC coupled with partitioned MPPT. Converters: 1. microinverter (MPPT), 2. battery inverter (BiD, CC), 3. load-packaged rectifier.

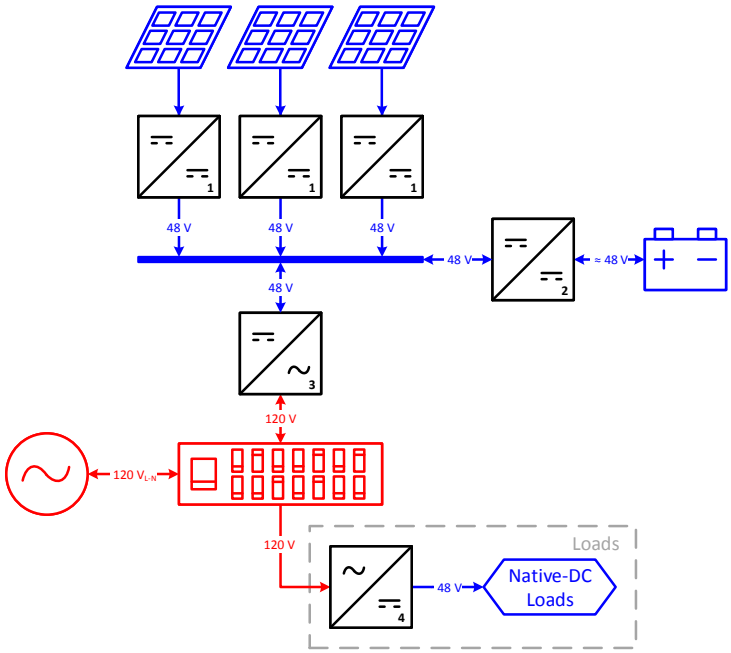

Figure B.14: Small office building network AC_{DC}': AC distribution DC coupled with partitioned MPPT. Converters: 1. power optimizer (MPPT), 2. battery charge controller (BiD, CC), 3. distribution inverter (BiD), 4. load-packaged rectifier.

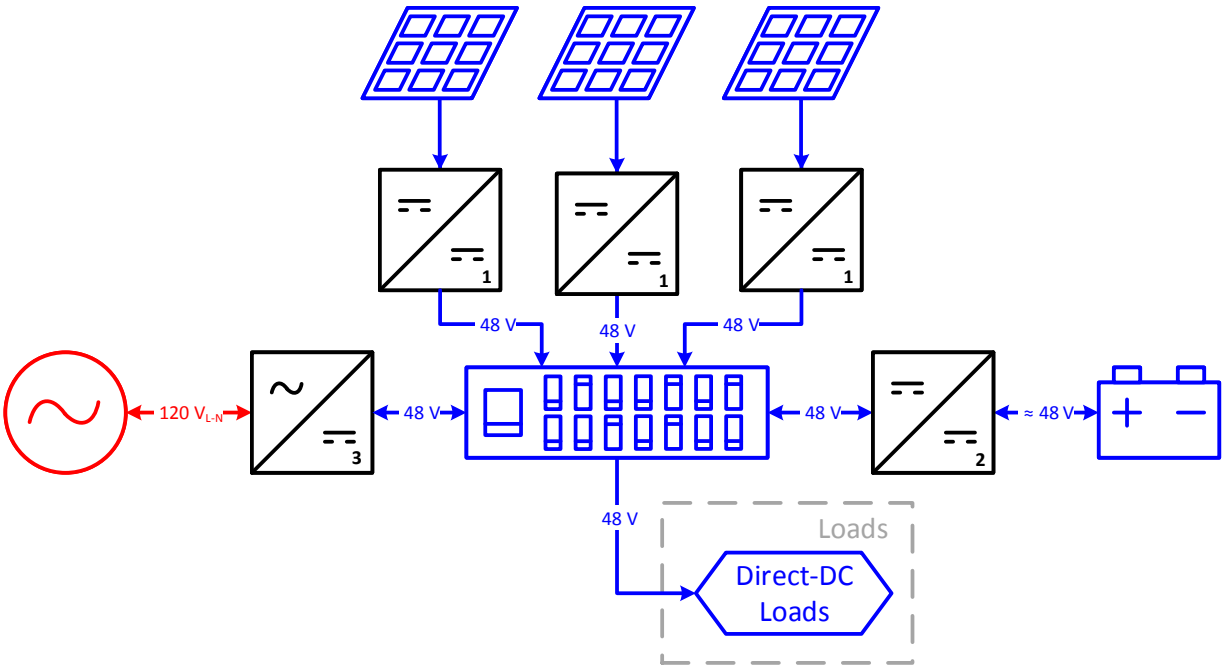

Figure B.15: Small office building network DC_{DC}': DC distribution DC coupled with partitioned MPPT. Converters: 1. power optimizer (MPPT), 2. battery charge controller (BiD, CC), 3. grid tie inverter (BiD). Certain loads such as LEDs require an additional DC-DC converter (not shown).

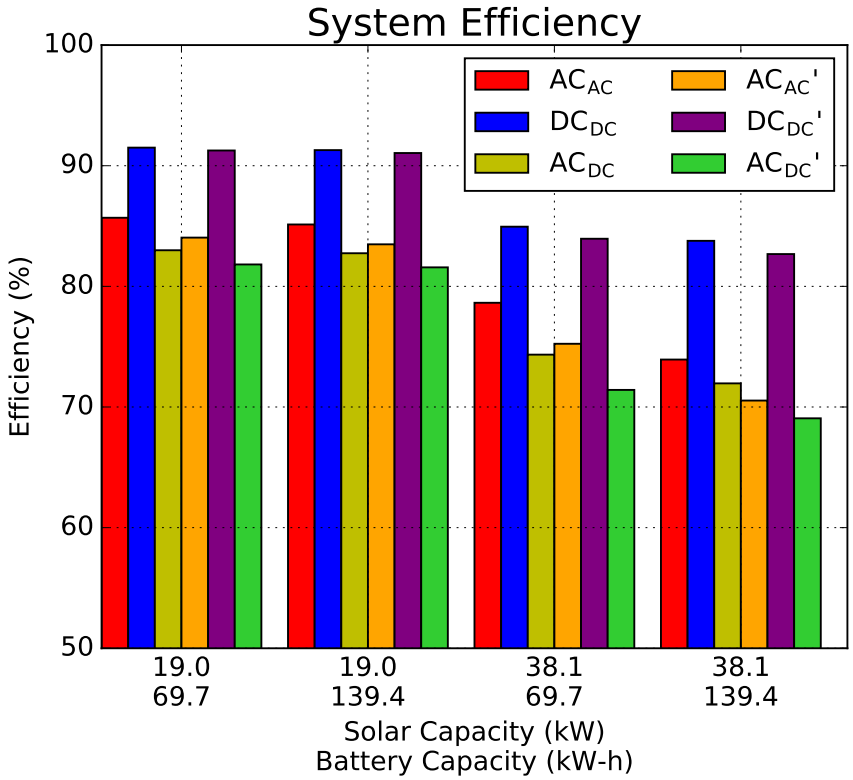

Figure B.16: Small office building simulation results for the topologies in Figures 2, 3 and B.12 to B.15.

a unified topology, the solar array is wired at the relatively high MPPT voltage. In a partitioned topology, the wire loss occurs after the MPPT conversion, at the much lower distribution voltage.

It is important to note that partitioned MPPT is very advantageous in PV systems that are prone to shading or soiling. Under such circumstances, partitioned MPPT systems can generate considerably more power than unified systems. This study does not account for the extra generation power.

There are several ways to reduce the wiring loss in partitioned MPPT systems. First, if the partitioned MPPT outputs at 380 V, the wiring loss will be mostly insignificant. In this case, the superior power optimizer efficiency may make partitioned MPPT more desirable for DC coupled systems. Second, the MPPT output wires in $AC_{AC}'$and DC_{DC}'can connect directly to the building distribution through the roof, thus greatly reducing overall wiring distance.

Appendix C. Large Office Building Simulation

The AC_{AC} and DC_{DC} network topologies are simulated in a large office building. The DC_{DC} topology is nearly identical to that of the medium office (Figure 5) except that the grid con-

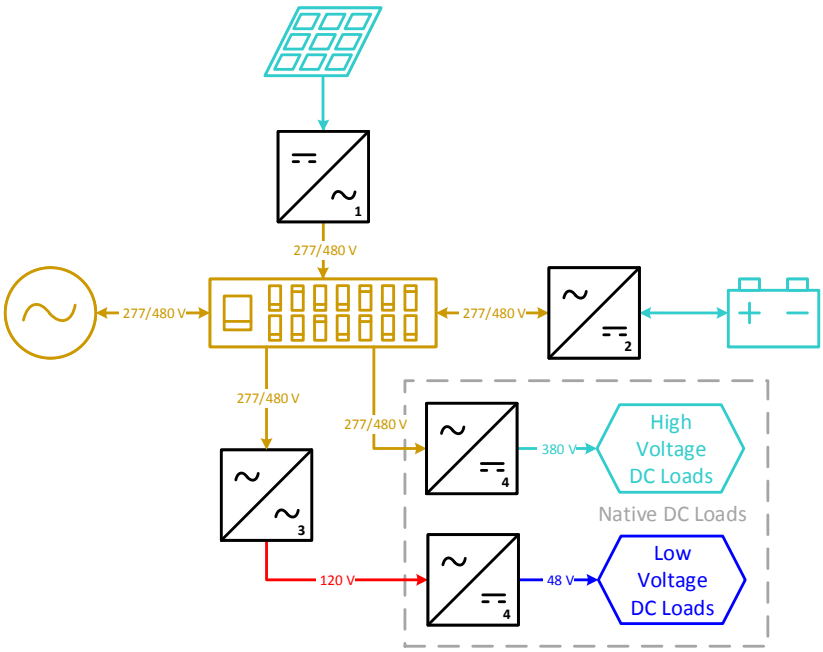

Figure C.17: Large office building network AC_{AC}: AC distribution AC coupled. Converters: 1. string or central inverter (MPPT), 2. battery inverter (BiD, CC), 3. transformer, 4. load-packaged rectifier.

nection is three-phase at 480 $V_{RMS,L\text{-}L}$. The AC_{AC} topology, shown in Figure C.17, uses a 480 $V_{RMS,L\text{-}L}$ backbone, which is standard for large buildings. Any loads or converters connected to this distribution backbone are assumed to be three-phase wye connected.

The large office building's load profile differs from that of the small and medium buildings. First, the large office building has a unique load profile for its elevators and data center. Second, the large office building uses central HVAC. The full HVAC model includes the electrical load profiles of a chiller, cooling tower, pumps, fans, humidifiers, and heating coils. The wiring to these loads is sized appropriately.

The simulation results for the large office building are summarized in Figure C.18. The efficiency savings with DC is generally less than in the medium office building. In the baseline case, the efficiency savings is 7.5%. The addition of a 480 $V_{RMS,L\text{-}L}$ backbone in the AC_{AC} network increases the conversion efficiency and decreases the wiring loss. In addition, AC-AC transformers are more efficient than high power DC-DC converters (both shown in blue in Figure C.18).

Finally, it is important to note the difficulty of implementing a large ZNE building. The modeled large office building has 13 floors [27–29]. Its roof can only fit 570.8 kW of solar capacity, which is roughly a tenth of that needed for the ZNE baseline. In general, rooftop solar works best on

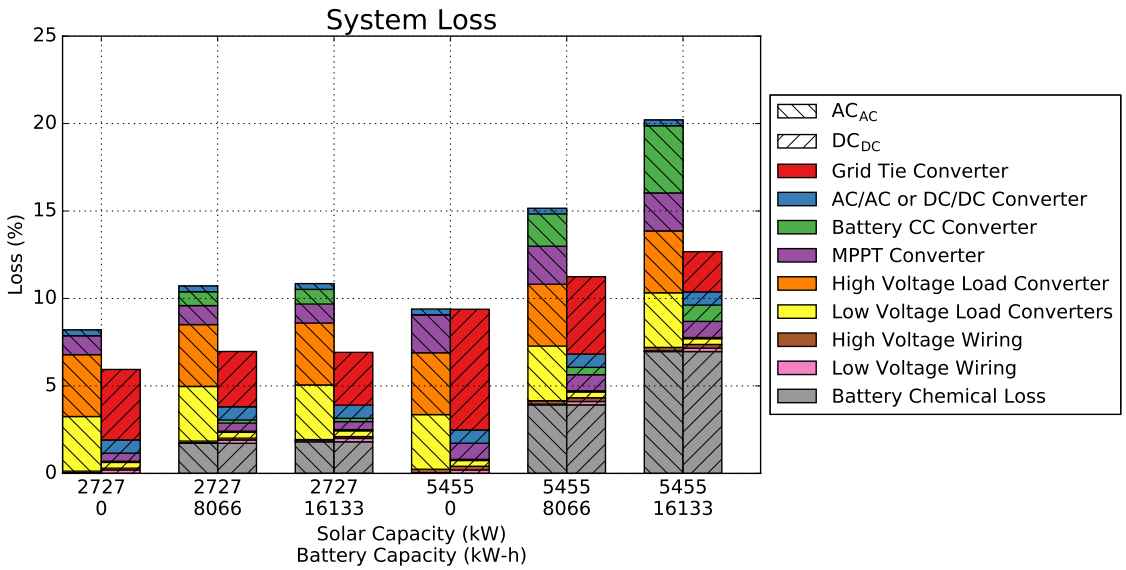

Figure C.18: Large office building loss analysis. Solar capacity is 50% and 100% of the baseline. Battery capacity is 0%, 50%, and 100% of the baseline.

short and wide buildings. Parking lots can be utilized, but the cost per kilowatt is more expensive due to the additional mechanical structure needed to support the solar panels above the parking. Nonetheless, parking canopies do provide added amenities and are easier to maintain than rooftop solar.

Overall, it is concluded that DC distribution is more beneficial for medium office buildings than for large office buildings.

Appendix D. Seasonal Simulations

Figure D.19 shows week-long simulations for the small office building that begin on the summer solstice or winter solstice. Solar generation varies considerably with season. HVAC usage in Los Angles is relatively light, and the load demand is somewhat less variant. In both seasons, the total load demand is very light on weekends and holidays. Although converter efficiency curves are affected by ambient temperature, seasonal temperature dependence is not included in the converter models.

For each seasonal simulation, the top transient plot shows that the peak solar generation and peak load demand are in phase. The middle plot shows how the battery controller charges and discharges the battery, depending on the amount of excess solar (Equation 1). The bottom plot shows when most of the losses occur during the week.

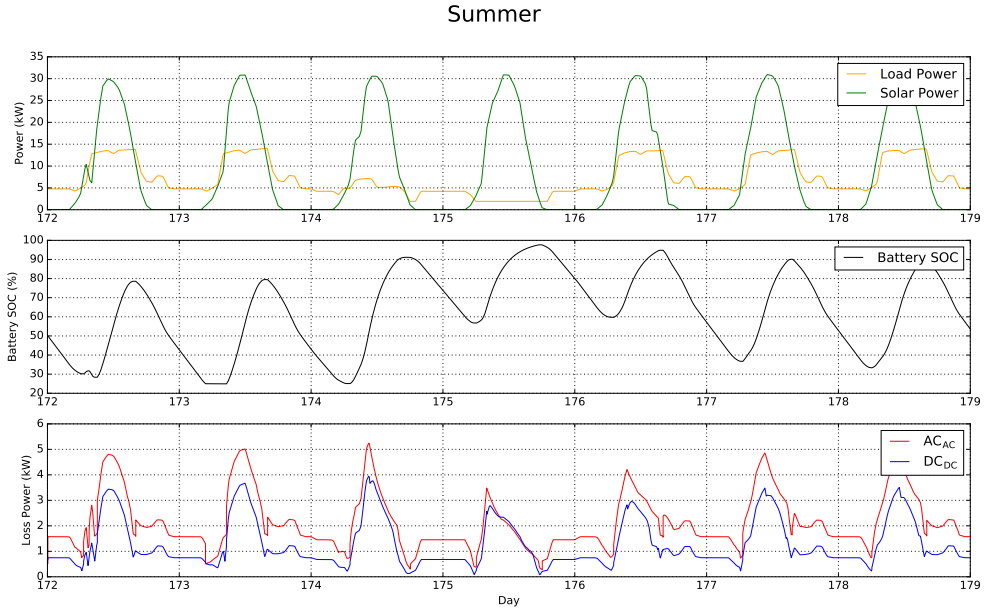

(a)

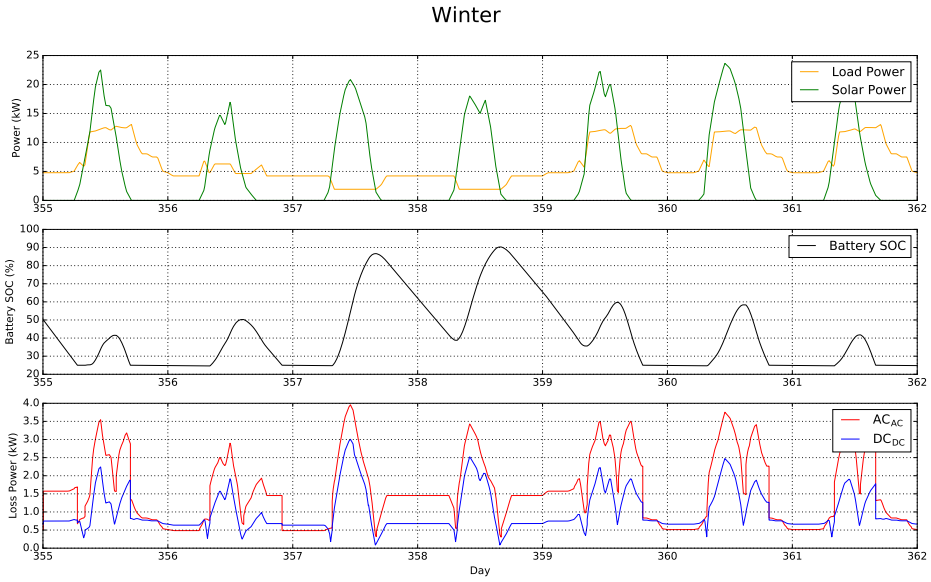

(b)

Figure D.19: Week-long simulations of the small office building during the (a) summer, and (b) winter.

Appendix E. Converter Efficiency Curves

The efficiency curves used in this study's product data are shown in Figures E.20 to E.22. The product categories may be labeled with "L" or "H," designating whether their inputs or outputs are low or high voltage. As described in Section 2, the DC voltage levels are 48 V and 380 V, and

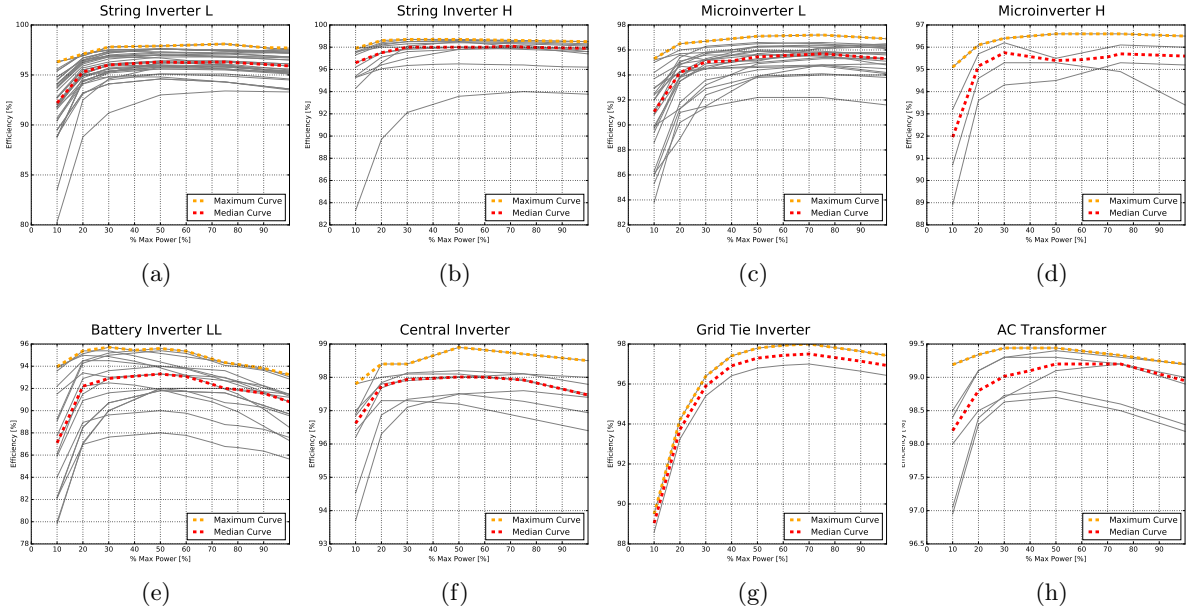

(a) (b) (c) (d)

(e) (f) (g) (h)

Figure E.20: Efficiency curves for inverters, bidirectional inverters, and transformers.

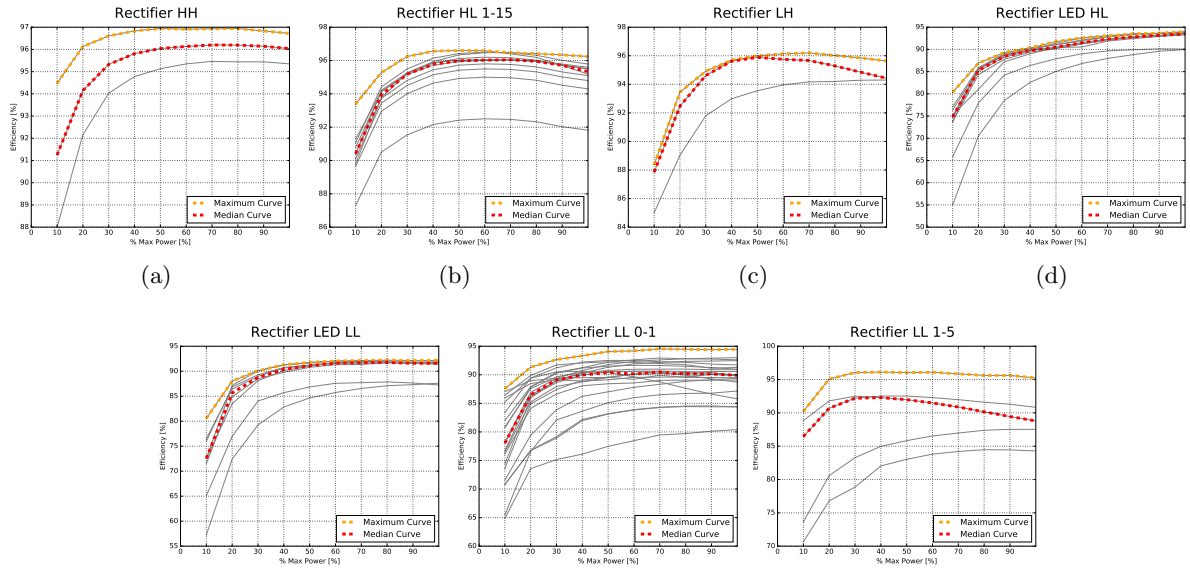

(a) (b) (c) (d)

(e) (f) (g)

Figure E.21: Efficiency curves for load rectifiers.

the AC levels are 120 V_{RMS} and 480 $V_{RMS,L\text{-}L}$. In addition, some of the product categories are labeled with a range of rated power (in kW).

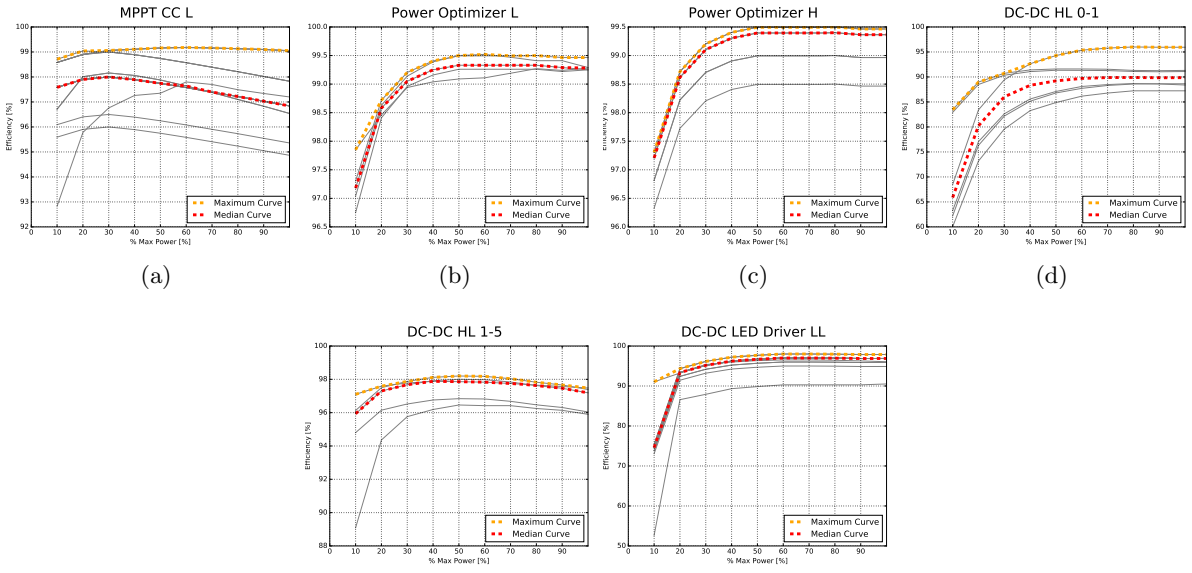

(a) (b) (c) (d)

(e) (f)

Figure E.22: Efficiency curves for all DC-DC converters.

Appendix F. Modelica Code Snapshot

Most of the Modelica simulation framework is based on the Buildings library [58, 59]. Many models are modified to support the needs of the efficiency study.

This is the Modelica code for battery charging algorithm discussed in Appendix Appendix A.2:

```
// set excess power, and charge/discharge rate
excessPower = SolarP - LoadP;
tauCharge = maxPower/(EMax*(1-SOCMin) + 0.01);
tauDischarge = maxPower/(EMax*SOCMax + 0.01);

// set charging or discharging power
if chargingState == 1 then // charging
  //powerLimit = maxPower;
  powerLimit = (1-SOC)*tauCharge*EMax;
  P = BuildingDC.Definitions.clamp(excessPower, 0, powerLimit);
elseif chargingState == -1 then // discharging
  //powerLimit = -maxPower;
  powerLimit = -(SOC)*tauDischarge*EMax;
  P = BuildingDC.Definitions.clamp(excessPower, powerLimit, 0);
else // hold charge state
  powerLimit = 0;
  P = 0;
end if;

// FSM for determining whether to charge, discharge, or hold
// sample(start, interval) in seconds
when sample(5*60, 30*60) then
```

```
    if disconnectBattery then
      chargingState = 0;
    else
      if pre(chargingState) == 1 then // currently charging
        if excessPower < chargingThreshold - hysteresisWidth then
          chargingState = -1; // discharge
        elseif SOC >= SOCMax then
          chargingState = 0; // hold
        else
          chargingState = 1; // charge
        end if;
      elseif pre(chargingState) == -1 then // currently discharging
        if excessPower > chargingThreshold + hysteresisWidth then
          chargingState = 1;
        elseif SOC <= SOCMin then
          chargingState = 0;
        else
          chargingState = -1;
        end if;
      else // currently holding charge state
        if excessPower > chargingThreshold + hysteresisWidth and
            SOC < SOCMax then
          chargingState = 1;
        elseif excessPower < chargingThreshold - hysteresisWidth
            and SOC > SOCMin then
          chargingState = -1;
        else
          chargingState = 0;
        end if;
      end if;
    end if;
  // set state to hold if SOC is outside its bounds
  elsewhen SOC > SOCMax or SOC < SOCMin then
    if SOC > SOCMax and pre(chargingState) == 1 then
      chargingState = 0;
    elseif SOC < SOCMin and pre(chargingState) == -1 then
      chargingState = 0;
    else
      chargingState = pre(chargingState);
    end if;
  end when;
```

This is the code for the wiring model discussed in Appendix Appendix A.3:

```
      // Determine average wire length based on the location
      //  of the hub (i.e. electrical room)
      if hubLocation == Types.HubLocation.Corner then
        avgWireLength = (width + length)/2;
      elseif hubLocation == Types.HubLocation.SideL then
        avgWireLength = (width + length/2)/2;
      elseif hubLocation == Types.HubLocation.SideW then
        avgWireLength = (width/2 + length)/2;
      else
        avgWireLength = (width/2 + length/2)/2;
```

```
    end if;
    // Determine number of units per floor of the particular
    //  load or end use
    if floorWiring == Types.FloorWiring.Perimeter then
      numUnitsPerFloor = floor(length/unitSpacing)*2 +
        floor(width/unitSpacing)*2;
    else
      numUnitsPerFloor = floor(length/unitSpacing)*
        floor(width/unitSpacing);
    end if;
    // Height adjustment to average wire length, depending
    //  on which and how many floors of the building have the
    //  particular load or end use
    if floorsUsed == Types.FloorsUsed.Basement then
      numUnits = numUnitsPerFloor;
      addHeightLength = 0;
    elseif floorsUsed == Types.FloorsUsed.MidFloors then
      if floors < 3 then
        numUnits = numUnitsPerFloor * floors;
      else
        numUnits = numUnitsPerFloor * (floors - 2);
      end if;
      addHeightLength = floors*heightPerFloor/2;
    elseif floorsUsed == Types.FloorsUsed.Roof then
      numUnits = numUnitsPerFloor;
      addHeightLength = floors*heightPerFloor;
    else // FloorsUsed.All
      numUnits = numUnitsPerFloor * floors;
      addHeightLength = floors*heightPerFloor/2;
    end if;
    // Determine total wire resistance based on
    //  average wire length, height adjustment, and
    //  the resistance per meter for this wire gauge
    if numUnits == 0 then
      RTotal = (avgWireLength + addHeightLength)*resPerM;
    else
      RTotal = (avgWireLength + addHeightLength)*
        resPerM/numUnits;
    end if;
```

References

[1] A. Perea, C. Honeyman, S. Kann, A. Mond, M. Shiao, S. Rumery, A. Holm, U.S. Solar Market Insight: 2016 Year in Review - Executive Summary, Tech. rep., GTM Research & Solar Energy Industries Association (Mar. 2017).

[2] G. Research, U.S. Energy Storage Monitor: Q4 2016 Executive Summary, Tech. rep., GTM Research (Dec. 2016).

[3] K. Garbesi, V. Vossos, H. Shen, Catalog of DC Appliances and Power Systems, Tech. Rep. LBNL-5364E, Lawrence Berkeley National Laboratory, Berkeley, CA (2011).

[4] K. George, DC Power Production, Delivery and Utilization: An EPRI White Paper.

[5] G. AlLee, W. Tschudi, Edison Redux: 380 Vdc Brings Reliability and Efficiency to Sustainable Data Centers, IEEE Power and Energy Magazine 10 (6) (2012) 50–59. doi:10.1109/MPE.2012.2212607.

[6] United States Energy Information Administration, 2012 Commercial Buildings Energy Consumption Survey: Energy Usage Summary, https://www.eia.gov/consumption/commercial/reports/2012/energyusage/, [Online; accessed 27-March-2017].

[7] N. P. Systems, Fort Belvoir Direct Coupling DC Microgrid.
URL http://www.nextekpower.com/fort-belvoir-direct-coupling-dc-microgrid/

[8] M. Wright, Eaton demonstrates distributed DC power for LED lighting at LFI, LEDs Magazine.
URL http://www.ledsmagazine.com/articles/2016/05/eaton-demonstrates-distributed-dc-power-for-led-lighting-a
html

[9] S. Backhaus, G. W. Swift, S. Chatzivasileiadis, W. Tschudi, S. Glover, M. Starke, J. Wang, M. Yue, D. Hammerstrom, DC Microgrids Scoping Study Estimate of Technical and Economic Benefits, Tech. Rep. LAUR1522097, Los Alamos National Laboratory (Mar. 2015).

[10] P. Savage, R. R. Nordhaus, S. P. Jamieson, From Silos to Systems: Issues in Clean Energy and Climate Change: DC microgrids: benefits and barriers, Tech. rep., Yale School of Forestry & Environmental Sciences (2010).

[11] D. Denkenberger, D. Driscoll, E. Lighthiser, P. May-Ostendorp, B. Trimboli, P. Walters, DC Distribution Market, Benefits, and Opportunities in Residential and Commercial Buildings, Tech. rep., Pacific Gas & Electric Company (Oct. 2012).

[12] A. Sannino, G. Postiglione, M. Bollen, Feasibility of a DC network for commercial facilities, IEEE Transactions on Industry Applications 39 (5) (2003) 1499–1507. doi:10.1109/TIA.2003.816517.

[13] B. A. Thomas, I. L. Azevedo, G. Morgan, Edison Revisited: Should we use DC circuits for lighting in commercial buildings?, Energy Policy 45 (2012) 399–411. doi:10.1016/j.enpol.2012.02.048.

[14] V. Vossos, K. Garbesi, H. Shen, Energy savings from direct-DC in U.S. residential buildings, Energy and Buildings 68, Part A (2014) 223–231. doi:10.1016/j.enbuild.2013.09.009.
URL http://www.sciencedirect.com/science/article/pii/S0378778813005720

[15] R. Weiss, L. Ott, U. Boeke, Energy efficient low-voltage DC-grids for commercial buildings, in: 2015 IEEE First International Conference on DC Microgrids (ICDCM), 2015, pp. 154–158. doi:10.1109/ICDCM.2015.7152030.

[16] U. Boeke, M. Wendt, DC power grids for buildings, in: 2015 IEEE First International Conference on DC Microgrids (ICDCM), 2015, pp. 210–214. doi:10.1109/ICDCM.2015.7152040.

[17] D. Fregosi, S. Ravula, D. Brhlik, J. Saussele, S. Frank, E. Bonnema, J. Scheib, E. Wilson, A comparative study of DC and AC microgrids in commercial buildings across different climates and operating profiles, in: 2015 IEEE First International Conference on DC Microgrids (ICDCM), 2015, pp. 159–164. doi:10.1109/ICDCM.2015.7152031.

[18] K. Engelen, E. Leung Shun, P. Vermeyen, I. Pardon, R. D'hulst, J. Driesen, R. Belmans, The Feasibility of Small-Scale Residential DC Distribution Systems, in: IECON 2006 - 32nd Annual Conference on IEEE Industrial Electronics, 2006, pp. 2618–2623. doi:10.1109/IECON.2006.347246.

[19] B. Glasgo, I. L. Azevedo, C. Hendrickson, How much electricity can we save by using direct current circuits in homes? Understanding the potential for electricity savings and assessing feasibility of a transition towards DC powered buildings, Applied Energy 180 (2016) 66–75. doi:10.1016/j.apenergy.2016.07.036.
URL http://www.sciencedirect.com/science/article/pii/S0306261916309771

[20] D. Hammerstrom, AC Versus DC Distribution Systems. Did We Get it Right?, in: IEEE Power Engineering Society General Meeting, 2007, 2007, pp. 1–5. doi:10.1109/PES.2007.386130.

[21] Z. Liu, M. Li, Research on Energy Efficiency of DC Distribution System, AASRI Procedia 7 (2014) 68–74. doi:10.1016/j.aasri.2014.05.031.
URL http://www.sciencedirect.com/science/article/pii/S2212671614000328

[22] M. Noritake, H. Hoshi, K. Hirose, H. Kita, R. Hara, M. Yagami, Operation algorithm of DC microgrid for achieving local production for local consumption of renewable energy, in: Telecommunications Energy Conference 'Smart Power and Efficiency' (INEC), Proceedings of 2013 35th International, 2013, pp. 1–6.

[23] M. Noritake, K. Yuasa, T. Takeda, H. Hoshi, K. Hirose, Demonstrative research on DC microgrids for office buildings, in: Telecommunications Energy Conference (INEC), 2014 IEEE 36th International, 2014, pp. 1–5. doi:10.1109/INTLEC.2014.6972180.

[24] P. Paajanen, T. Kaipia, J. Partanen, DC supply of low-voltage electricity appliances in residential buildings, in: CIRED 2009 - 20th International Conference and Exhibition on Electricity Distribution - Part 1, 2009, pp. 1–4. doi:10.1049/cp.2009.0925.

[25] M. Starke, L. Tolbert, B. Ozpineci, AC vs. DC distribution: A loss comparison, in: Transmission and Distribution Conference and Exposition, 2008. T #x00026;D. IEEE/PES, 2008, pp. 1–7. doi:10.1109/TDC.2008.4517256.

[26] S. Willems, W. Aerts, Study and Simulation Of A DC Micro Grid With Focus on Efficiency, Use of Materials and Economic Constraints, Ph.D. thesis, University of Leuven, Leuven, Belgium (2014).
URL http://www.dehaagsehogeschool.nl/xmsp/xms_itm_p.download_file?p_itm_id=94657

[27] M. Deru, K. Field, D. Studer, K. Benne, B. Griffith, P. Torcellini, B. Liu, M. Halverson, D. Winiarski, M. Rosenberg, et al., US Department of Energy commercial reference building models of the national building stock.

[28] NREL, PNNL and LBNL, US, Department of energy, commercial reference building models of the national building stock, Tech. rep., Technical Report NREL/TP-5500-46861 (2011).
[29] U.S. Department of Energy, Commercial reference buildings, https://energy.gov/eere/buildings/commercial-reference-buildings, [Online; accessed 10-March-2017] (2017).
[30] F. G. Osorio, M. Xinran, Y. Liu, P. Lusina, E. Cretu, Sensor network using power-over-ethernet, in: Computing and Communication (IEMCON), 2015 International Conference and Workshop on, IEEE, 2015, pp. 1–7.
[31] J. Petroski, Power over ethernet thermal analysis with an engineering mechanics approach, in: Thermal Measurement, Modeling & Management Symposium (SEMI-THERM), 2016 32nd, IEEE, 2016, pp. 50–56.
[32] J. Johnston, J. Counsell, G. Banks, M. J. Stewart, Beyond power over ethernet: The development of digital energy networks for buildings, in: CIBSE Technical Symposium 2012-Buildings Systems and Services for the 21st Century, 2012, pp. Session–5.
[33] E. Alliance, 380 Vdc Architectures for the Modern Data Center, EMerge Alliance, San Ramon, CA, USA.
[34] D. E. Geary, D. P. Mohr, D. Owen, M. Salato, B. Sonnenberg, 380V DC eco-system development: present status and future challenges, in: Telecommunications Energy Conference'Smart Power and Efficiency'(INTELEC), Proceedings of 2013 35th International, VDE, 2013, pp. 1–6.
[35] D. J. Becker, B. Sonnenberg, DC microgrids in buildings and data centers, in: Telecommunications Energy Conference (INTELEC), 2011 IEEE 33rd International, IEEE, 2011, pp. 1–7.
[36] NREL, A performance calculator for grid-connected pv systems (2010).
[37] National Renewable Energy Lab, PVWatts Calculator, http://pvwatts.nrel.gov/pvwatts.php, [Online; accessed 10-March-2017] (2017).
[38] D. Freeman, Introduction to photovoltaic systems maximum power point tracking, Texas Instruments Application Report SLVA446.
[39] W. Xiao, N. Ozog, W. G. Dunford, Topology study of photovoltaic interface for maximum power point tracking, IEEE Transactions on Industrial Electronics 54 (3) (2007) 1696–1704.
[40] California Energy Commission & California Public Utilities Commission, Go solar california, http://www.gosolarcalifornia.org/equipment/inverter_tests/summaries/ (2007).
[41] E. Hittinger, T. Wiley, J. Kluza, J. Whitacre, Evaluating the value of batteries in microgrid electricity systems using an improved energy systems model, Energy Conversion and Management 89 (2015) 458–472.
[42] Y. Ru, J. Kleissl, S. Martinez, Storage size determination for grid-connected photovoltaic systems, IEEE Transactions on Sustainable Energy 4 (1) (2013) 68–81.
[43] B. S. Borowy, Z. M. Salameh, Methodology for optimally sizing the combination of a battery bank and PV array in a wind/PV hybrid system, IEEE Transactions on energy conversion 11 (2) (1996) 367–375.
[44] L. Xu, X. Ruan, C. Mao, B. Zhang, Y. Luo, An improved optimal sizing method for wind-solar-battery hybrid power system, IEEE transactions on Sustainable Energy 4 (3) (2013) 774–785.
[45] W. Shen, Optimally sizing of solar array and battery in a standalone photovoltaic system in malaysia, Renewable energy 34 (1) (2009) 348–352.
[46] C. Protogeropoulos, B. Brinkworth, R. Marshall, Sizing and techno-economical optimization for hybrid solar photovoltaic/wind power systems with battery storage, International Journal of Energy Research 21 (6) (1997) 465–479.
[47] A. J. Marszal, P. Heiselberg, J. S. Bourrelle, E. Musall, K. Voss, I. Sartori, A. Napolitano, Zero energy building–a review of definitions and calculation methodologies, Energy and buildings 43 (4) (2011) 971–979.
[48] S. Pless, P. Torcellini, Getting to net zero, ASHRAE Journal 51 (9) (2009) 18.
[49] S. Attia, M. Hamdy, W. OBrien, S. Carlucci, Assessing gaps and needs for integrating building performance optimization tools in net zero energy buildings design, Energy and Buildings 60 (2013) 110–124.
[50] K. Voss, I. Sartori, A. Napolitano, S. Geier, H. Gonçalves, M. Hall, P. Heiselberg, J. Widén, J. A. Candanedo, E. Musall, et al., Load matching and grid interaction of net zero energy buildings, in: EUROSUN 2010 International Conference on Solar Heating, Cooling and Buildings, 2010.
[51] R. L. Fares, M. E. Webber, The impacts of storing solar energy in the home to reduce reliance on the utility, Nature Energy 2 (2017) 17001.
[52] K. Divya, J. Østergaard, Battery energy storage technology for power systems: An overview, Electric Power Systems Research 79 (4) (2009) 511–520.
[53] M. Stadler, M. Kloess, M. Groissböck, G. Cardoso, R. Sharma, M. C. Bozchalui, C. Marnay, Electric storage in California's commercial buildings, Applied Energy 104 (2013) 711–722.
[54] E. Hittinger, J. Siddiqui, The challenging economics of US residential grid defection, Utilities Policy.
[55] M. Jin, W. Feng, P. Liu, C. Marnay, C. Spanos, MOD-DR: Microgrid optimal dispatch with demand response, Applied Energy 187 (2017) 758–776.

[56] National Fire Protection Association and others, NFPA 70: National Electric Code, Quincy, MA.
[57] Schneider Electric, AC Coupling of Inverters, rev. D (6 2015).
[58] M. Wetter, W. Zuo, T. S. Nouidui, X. Pang, Modelica buildings library, Journal of Building Performance Simulation 7 (4) (2014) 253–270.
[59] M. Bonvini, M. Wetter, T. Noudui, A modelica package for buildings-to-electrical grid integration, in: Proc. of Fifth German-Austrian IBPSA Conference, Vol. 1, 2014, pp. 6–13.